

## Investigating the observational properties of Type Ib supernova SN 2017iro

BRAJESH KUMAR <sup>1,2</sup>, AVINASH SINGH <sup>3,2</sup>, D.K. SAHU <sup>2</sup>, AND G.C. ANUPAMA <sup>2</sup>

<sup>1</sup>*Aryabhata Research Institute of Observational Sciences, Manora Peak, Nainital - 263001, India*

<sup>2</sup>*Indian Institute of Astrophysics, II Block, Koramangala, Bengaluru 560034, India*

<sup>3</sup>*Hiroshima Astrophysical Science Center, Hiroshima University, Higashi-Hiroshima, Hiroshima 739-8526, Japan*

(Received –; Revised –; Accepted –)

Submitted to ApJ

### ABSTRACT

We report results of optical imaging and low-resolution spectroscopic monitoring of supernova (SN) 2017iro that occurred in the nearby ( $\sim 31$  Mpc) galaxy NGC 5480. The He I 5876 Å feature present in the earliest spectrum ( $-7$  d) classified it as a Type Ib SN. The follow-up observations span from  $-7$  to  $+266$  d with respect to the  $B$ -band maximum. With a peak absolute magnitude in  $V$ -band,  $(M_V) = -17.76 \pm 0.15$  mag and bolometric luminosity  $(\log_{10} L) = 42.39 \pm 0.09$  erg  $s^{-1}$ , SN 2017iro is a moderately luminous Type Ib SN. The overall light curve evolution of SN 2017iro is similar to SN 2012au and SN 2009jf during the early (up to  $\sim 100$  d) and late phases ( $>150$  d), respectively. The line velocities of both Fe II 5169 Å and He I 5876 Å are  $\sim 9000$  km  $s^{-1}$  near the peak. The analysis of the nebular phase spectrum ( $\sim +209$  d) indicates an oxygen mass of  $\sim 0.35 M_{\odot}$ . The smaller [O I]/[Ca II] flux ratio of  $\sim 1$  favours a progenitor with a zero-age main-sequence mass in the range  $\sim 13$ – $15 M_{\odot}$ , most likely in a binary system, similar to the case of iPTF13bvn. The explosion parameters are estimated by applying different analytical models to the quasi-bolometric light curve of SN 2017iro.  $^{56}\text{Ni}$  mass synthesized in the explosion has a range of  $\sim 0.05$ – $0.10 M_{\odot}$ , the ejecta mass  $\sim 1.4$ – $4.3 M_{\odot}$  and the kinetic energy  $\sim 0.8$ – $1.9 \times 10^{51}$  erg.

*Keywords:* supernovae: general – supernovae: individual: SN 2017iro, galaxies: individual: NGC 5480

### 1. INTRODUCTION

Type Ib, Ic, Ic-broad lined (Ic-BL), and IIb supernovae (SNe) belong to the class of stripped-envelope supernovae (SE-SNe, Minkowski 1941; Clocchiatti & Wheeler 1997; Filippenko 1997; Gal-Yam 2017; Modjaz et al. 2019). SE-SNe are generally characterized by bell-shaped light curves (LCs) which are mainly powered by the thermal energy released as a consequence of radioactive decay of the iron group elements ( $^{56}\text{Ni} \rightarrow ^{56}\text{Co} \rightarrow ^{56}\text{Fe}$ ) synthesized in the explosion. SE-SNe show no hydrogen (Ib) or neither hydrogen nor helium (Ic) in their spectra except for Type IIb events, which exhibit hydrogen in the early phase spectra (Filippenko 1988; Filippenko, Matheson, & Ho 1993). This indicates that they are the results of explosion of stars that are devoid of the outer layer of hydrogen (Ib) or both hy-

drogen and helium (Ic) at the time of explosion. The spectroscopic behaviour of SE-SNe separates them from Type II SNe, where hydrogen is found to be dominant in the spectra. The SE-SNe and Type II events are collectively grouped as core-collapse supernovae (CC-SNe) as they result from the gravitational collapse of the iron core of massive stars ( $M \geq 8 M_{\odot}$ ) during the end stages of their lives (Heger et al. 2003; Smartt 2009).

In SE-SNe, the mechanisms responsible for removing the outer envelopes (hydrogen or helium) of the progenitors can be either radiation-driven stellar winds (Conti 1975; Puls, Vink, & Najarro 2008; Pauldrach, Vanbeveren, & Hoffmann 2012), eruptive mass loss (Smith & Owocki 2006; Smith 2006) and/or mass transfer to a companion star (Nomoto 1984, 1987; Wheeler & Livereault 1985; Podsiadlowski, Joss, & Hsu 1992; Woosley & Weaver 1995; Nomoto, Iwamoto, & Suzuki 1995; Wellstein & Langer 1999; Wellstein, Langer, & Braun 2001; Pols & Dewi 2002; Podsiadlowski, Langer, Poelarends, Rappaport, Heger, & Pfahl 2004; Yoon, Woosley, & Langer 2010). Depending on the main-sequence mass

of the progenitor star, above mechanisms or a combination of them operates. In the case of a single massive ( $> 20 M_{\odot}$ ) Wolf-Rayet star, the radiation-driven stellar wind is the dominant process (see Woosley et al. 1995; Massey 2003; Crowther 2007; Smith 2014a; Yoon 2015a, and references therein). In case of moderately massive ( $8-25 M_{\odot}$ ) stars, mass transfer to the binary companion effectively removes the outer envelope (Groh, Georgy, & Ekström 2013a,b; Smith 2014b; Yoon 2015b, and references therein).

Dedicated and large area transient survey programmes have made it possible to discover a large number of SNe of different types. The SE-SNe constitute a reasonable fraction ( $\sim 25-30\%$ ) of the overall SN rate in the local Universe (Li et al. 2011a; Eldridge et al. 2013; Graur et al. 2017a,b). The availability of ample data has led to a qualitative analysis of a large sample of SE-SNe in the recent years (see, e.g. Drout et al. 2011; Bianco et al. 2014; Modjaz et al. 2014a; Taddia et al. 2015; Liu et al. 2016; Lyman et al. 2016; Prentice et al. 2016; Taddia et al. 2018; Prentice et al. 2019; Shivvers et al. 2019; Williamson et al. 2019; Shahbandeh et al. 2021). These studies reveal that heterogeneity exists in the observational properties of SE-SNe in terms of synthesized  $^{56}\text{Ni}$  masses ( $\sim 0.1-0.4 M_{\odot}$ ), ejecta masses ( $\sim 1-6 M_{\odot}$ ), explosion energies (few  $10^{51}$  erg), and absolute magnitude ( $\sim -17$  to  $-18$  mag). Notably, the sample selection criteria and the methods applied may induce inconsistency in various estimates (see, Taddia et al. 2018; Prentice et al. 2019).

Statistical investigations of a large sample of photometric data are useful in exploring the bulk properties of various types of events. Nevertheless, such studies are generally limited to LCs in selected pass-bands, and also, the follow-up covers a short duration of the SN evolution. Further, the spectroscopic follow-up of most objects is restricted to early phases. Non-uniformity in the data sample may also be present as these are collected at different observing facilities and detectors. Studying individual events with proper monitoring at different phases (both photospheric and nebular) is hence extremely important. The very early phase observations (hours to days after explosion) of these events are useful to constrain the progenitor radius at its end stage. This needs a very early detection and quick follow up which is not always possible considering their random occurrence in the sky. The large area surveys with high cadence have contributed significantly in this regard. SN 1993J (Type IIb) is the first event among SE-SNe which shows evidence of a prominent cooling tail just after explosion (Richmond et al. 1994; Barbon et al. 1995). During last two decades several Type IIb SNe with such interesting features have been monitored and studied well e.g. SN 2008ax (Pastorello et al. 2008; Roming et al. 2009), SN 2011dh (Arcavi et al. 2011), SN 2011fu (Kumar et al. 2013; Morales-Garoffolo et al. 2015), SN 2013df (Fremling et al. 2014) and SN 2016gkg (Arcavi et al.

2017; Tartaglia et al. 2017a). A handful of Type Ib events have also been discovered at very early phases and their observational properties are studied in detail such as SN 1999ex (Hamuy et al. 2002; Stritzinger et al. 2002), SN 2008D (Soderberg et al. 2008; Mazzali et al. 2008; Malesani et al. 2009; Modjaz et al. 2009a; Bersten et al. 2013), iPTF13bvn (Fremling et al. 2016; Bersten et al. 2014a) and LSQ13abf (Stritzinger et al. 2020). Recently, Prentice et al. (2019) analyzed the properties of 18 SE-SNe and discussed the implications for their progenitors. Direct detection of SE-SNe progenitor candidates has been possible only for a few objects, e.g. SN 1993J (Maund et al. 2004), SN 2011dh (Maund et al. 2011; Van Dyk et al. 2013), SN 2001ig (Ryder et al. 2018), iPTF13bvn (Cao et al. 2013; Eldridge et al. 2015a; Kuncarayakti et al. 2015a; Folatelli et al. 2016), SN 2016gkg (Kilpatrick et al. 2017; Tartaglia et al. 2017a), SN 2017ein (Kilpatrick et al. 2018; Van Dyk et al. 2018; Xiang et al. 2019) and SN 2019yvr (Kilpatrick et al. 2021). Along with very early phases, the temporal observations during maximum to nebular phases are equally important to estimate various explosion parameters and progenitor properties. Detail investigation of more events can provide an alternative way to understand various progenitor channels.

SN 2017iro was discovered by Patrick Wiggins on 2017 November 30.5 UT (Wiggins 2017) at about 15 arcsec South-East of the centre of the galaxy NGC 5480 which also hosted another Type Ib event SN 1988L (Perlmutter et al. 1988). Pre-explosion images of host galaxy, obtained by *Hubble Space Telescope* (HST) in F606W-band using Wide Field Camera (WFC) of Advanced Camera for Surveys (ACS), exist in the HST archive. SN 2017iro was discovered at a magnitude of  $\sim 15.5$  mag (clear filter) and classified as a Type Ib/c SN with the help of the spectrum taken on 2017 December 02 (Bertrand 2017). To be noted that SN 2017iro discovery was slightly late ( $\sim 8$  d after explosion) however, we were able to cover its peak as well as the late phase observations with a good sampling of photometric and spectroscopic data points. Table 1 lists details of SN 2017iro and its host galaxy.

Results based on well-sampled optical photometric and low-resolution spectroscopic observations of SN 2017iro are presented in this paper. The observations and data reduction are described in Section 2. Light curve and spectral properties are presented in Section 3 and 4, respectively. In Section 5, the results are discussed, and the summary is provided in Section 6.

## 2. OBSERVATIONS AND DATA REDUCTION

### 2.1. Photometric observation

The photometric follow-up of SN 2017iro started just after the announcement of its discovery, i.e., 2017 December 01 (JD 2458089.5), and continued up to 2018 August 31 (JD 2458362.1). These observations were performed in Bessell *UBVRI* bands with the Himalayan Faint Object Spectrograph Camera (HFOSC), mounted

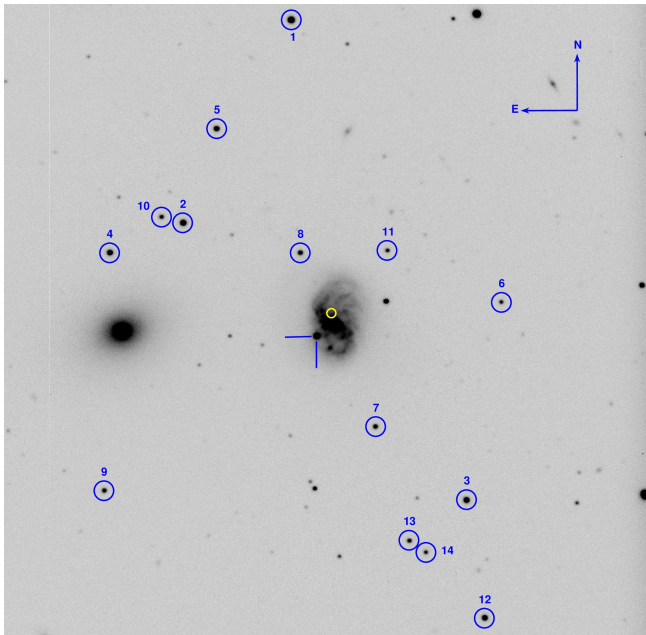


**Figure 1.** Identification chart of SN 2017iro obtained in V-band (SN is marked with blue crosshairs). The field of view is roughly  $9 \text{ arcmin} \times 9 \text{ arcmin}$ . The IDs 1–14 indicate secondary standard stars in the SN field (their magnitudes are listed in Table 2). The location of SN 1988L is also marked with a bold circle (yellow).

**Table 1.** Details of SN 2017iro and its host galaxy.

Parameters	Value	Reference
SN 2017iro:		
RA (J2000)	$14^{\text{h}} 06^{\text{m}} 23^{\text{s}}.11$	1
DEC (J2000)	$+50^{\circ} 43' 20''.20$	1
Explosion epoch (UT)	2017 November 23 (JD 2458080.7)	Section 3.1
Discovery date (UT)	2017 November 30.5 (JD 2458088.0)	1
$E(B - V)_{\text{total}}$	$0.28 \pm 0.04 \text{ mag}$	Section 3.3
NGC 5480:		
Type	SA(s)c	2
Redshift	$0.006191 \pm 0.000017$	2
Distance	$30.8 \pm 2.2 \text{ Mpc}$	3
Distance modulus	$32.44 \pm 0.15 \text{ mag}$	3

<sup>1</sup> <https://wis-tns.weizmann.ac.il/object/2017iro>

<sup>2</sup> NASA/IPAC Extragalactic Database (NED)

<sup>3</sup> Mould et al. (2000)

on the  $f/9$  Cassegrain focus of the 2 m Himalayan Chandra Telescope (HCT) of Indian Astronomical Observatory (IAO), Hanle, India (Prabhu 2014). HFOSC is equipped with a liquid nitrogen-cooled  $2\text{k} \times 4\text{k}$  pixels SITe CCD chip (pixel size  $15 \times 15 \mu\text{m}$ ). The gain and readout noise of the detector are  $1.22 \text{ e}^-/\text{ADU}$  and  $4.87 \text{ e}^-$ , respectively. With a plate scale of  $0.296 \text{ arcsec}$  per pixel, the central  $2\text{k} \times 2\text{k}$  region covers a field of  $10' \times 10'$  on the sky and is used for imaging. Further description

on the HCT and the HFOSC instrument can be obtained from [https://www.iap.res.in/?q=iao\\_about](https://www.iap.res.in/?q=iao_about).

During the observations, several bias and twilight flat frames were obtained along with science frames. The usual pre-processing steps, such as bias-subtraction, flat-fielding correction, and cosmic ray removal, were applied to raw images of the SN. For this purpose, standard tasks available in the data reduction software IRAF<sup>1</sup> were used. In order to achieve a better signal-to-noise ratio, multiple frames were taken on some nights and co-added in respective bands after the alignment of the images.

To calibrate a sequence of secondary standards in the SN field, we observed Landolt photometric standard fields (Landolt 1992) PG0231+051, PG0918+029, PG0942-029, and PG1047+003 on three nights, 2018, January 21, February 03 and 25, under good photometric conditions along with the SN field. The observed Landolt field stars cover a brightness range of  $12.27 \leq V \leq 16.11 \text{ mag}$  and colour range of  $-0.33 \leq B - V \leq 1.45 \text{ mag}$ . The average atmospheric extinction values in  $U$ ,  $B$ ,  $V$ ,  $R$  and  $I$  bands for the site were adopted from Stalin et al. (2008). The average colour terms for the telescope detector system were used to determine the photometric zero-points by applying a linear relationship between the observed and standard colours. A set of 14 stars in the SN field (marked in Fig. 1), were calibrated using the estimated zero-points and average colour terms. The calibrated  $UBVRI$  magnitudes of the secondary standards averaged over three nights are listed in Table 2. Considering the proximity of SN to an H II region, template subtraction was performed using the template images of the host galaxy, observed on 2019 August 21 with the HCT. The instrumental magnitudes of the supernova at different epochs were extracted from the template subtracted images. The SN magnitude is calibrated differentially with respect to the secondary standards in the SN field by applying the nightly zero points (see Kumar et al. 2018). The photometric magnitudes of SN along with the errors are listed in Table 3. Here, photometric errors include the errors in aperture photometry as estimated in IRAF and uncertainties in the nightly zero points, added in quadrature.

## 2.2. Spectroscopic observation

Low-resolution optical spectroscopic observations of SN 2017iro were obtained at 34 epochs during 2017 December 01 (JD 2458089.4) to 2018 July 05 (JD 2458305.2). Two grisms Gr#7 ( $3500\text{--}7800 \text{ \AA}$ ) and Gr#8 ( $5200\text{--}9250 \text{ \AA}$ ) available with HFOSC, were used to obtain the SN 2017iro spectra. The spectra of arc

<sup>1</sup> IRAF stands for Image Reduction and Analysis Facility. It is distributed by the National Optical Astronomy Observatory, which is operated by the Association of Universities for Research in Astronomy (AURA) under a cooperative agreement with the National Science Foundation.

**Table 2.** Calibrated magnitudes of secondary standards in the field of SN 2017iro. Star IDs are indicated in Fig. 1.

Star ID	<i>U</i> (mag)	<i>B</i> (mag)	<i>V</i> (mag)	<i>R</i> (mag)	<i>I</i> (mag)
1	15.86 ± 0.07	15.93 ± 0.02	15.34 ± 0.01	14.95 ± 0.02	14.56 ± 0.01
2	16.16 ± 0.06	16.39 ± 0.01	15.87 ± 0.01	15.53 ± 0.02	15.20 ± 0.01
3	18.02 ± 0.02	17.21 ± 0.02	16.21 ± 0.01	15.59 ± 0.01	15.07 ± 0.01
4	18.09 ± 0.09	17.26 ± 0.01	16.22 ± 0.01	15.57 ± 0.02	15.00 ± 0.01
5	17.21 ± 0.06	17.10 ± 0.01	16.41 ± 0.01	15.97 ± 0.02	15.54 ± 0.01
6	19.83 ± 0.05	19.33 ± 0.05	17.85 ± 0.02	16.50 ± 0.02	14.91 ± 0.02
7	17.62 ± 0.01	17.74 ± 0.01	17.14 ± 0.01	16.76 ± 0.02	16.41 ± 0.02
8	17.33 ± 0.04	17.51 ± 0.02	16.95 ± 0.02	16.59 ± 0.03	16.24 ± 0.03
9	18.14 ± 0.02	17.96 ± 0.01	17.23 ± 0.01	16.78 ± 0.02	16.38 ± 0.01
10	19.92 ± 0.69	18.90 ± 0.04	17.48 ± 0.02	16.30 ± 0.02	14.92 ± 0.01
11	18.27 ± 0.01	18.33 ± 0.02	17.68 ± 0.02	17.28 ± 0.02	16.84 ± 0.06
12	18.17 ± 0.05	17.36 ± 0.01	16.40 ± 0.01	15.80 ± 0.02	15.29 ± 0.01
13	18.04 ± 0.01	18.11 ± 0.01	17.51 ± 0.01	17.12 ± 0.02	16.74 ± 0.01
14	18.66 ± 0.02	18.52 ± 0.02	17.80 ± 0.02	17.36 ± 0.03	16.95 ± 0.03

**Table 3.** Log of photometric observations and estimated *UBVRI* magnitudes of SN 2017iro.

Date (yyyy-mm-dd)	JD 2450000+	Phase* (d)	<i>U</i> (mag)	<i>B</i> (mag)	<i>V</i> (mag)	<i>R</i> (mag)	<i>I</i> (mag)
2017-12-01	8089.5	-6.7	15.85 ± 0.11	16.29 ± 0.03	16.01 ± 0.11	15.78 ± 0.04	15.67 ± 0.07
2017-12-02	8090.5	-5.7	15.71 ± 0.11	16.20 ± 0.13	15.93 ± 0.11	15.71 ± 0.03	15.56 ± 0.08
2017-12-05	8093.4	-2.8	15.64 ± 0.11	15.96 ± 0.13	15.68 ± 0.05	15.47 ± 0.09	15.33 ± 0.11
2017-12-06	8094.4	-1.8	15.64 ± 0.11	16.01 ± 0.09	15.63 ± 0.11	15.38 ± 0.05	15.21 ± 0.07
2017-12-07	8095.5	-0.7	15.63 ± 0.12	15.95 ± 0.05	15.56 ± 0.03	15.25 ± 0.02	15.118 ± 0.03
2017-12-08	8096.5	+0.3	15.68 ± 0.12	15.92 ± 0.06	15.56 ± 0.10	15.22 ± 0.10	15.10 ± 0.13
2017-12-09	8097.5	+1.3	-	-	15.52 ± 0.02	15.20 ± 0.03	15.06 ± 0.03
2017-12-12	8100.5	+4.3	15.84 ± 0.12	16.12 ± 0.11	15.58 ± 0.01	15.19 ± 0.04	14.99 ± 0.06
2017-12-14	8102.5	+6.3	-	16.33 ± 0.05	15.69 ± 0.04	15.19 ± 0.02	14.96 ± 0.08
2017-12-17	8105.4	+9.2	17.00 ± 0.13	16.74 ± 0.03	15.84 ± 0.05	15.32 ± 0.02	15.06 ± 0.04
2017-12-26	8114.4	+18.2	18.50 ± 0.14	17.76 ± 0.04	16.43 ± 0.02	15.81 ± 0.04	15.38 ± 0.04
2017-12-29	8117.4	+21.2	-	-	16.61 ± 0.02	15.98 ± 0.02	15.59 ± 0.02
2018-01-05	8124.5	+28.3	-	18.28 ± 0.04	16.90 ± 0.06	16.27 ± 0.02	15.77 ± 0.07
2018-01-07	8126.4	+30.2	19.07 ± 0.14	-	16.96 ± 0.10	16.32 ± 0.08	15.84 ± 0.07
2018-01-08	8127.4	+31.2	-	-	16.96 ± 0.06	16.25 ± 0.11	15.79 ± 0.09
2018-01-14	8133.4	+37.2	-	18.40 ± 0.03	17.14 ± 0.01	16.51 ± 0.02	15.99 ± 0.03
2018-01-16	8135.4	+39.2	19.10 ± 0.20	18.50 ± 0.04	17.21 ± 0.02	16.57 ± 0.04	16.03 ± 0.06
2018-01-17	8136.5	+40.3	-	18.52 ± 0.06	17.24 ± 0.02	16.62 ± 0.02	16.05 ± 0.05
2018-01-21	8140.4	+44.2	-	18.49 ± 0.03	17.31 ± 0.02	16.72 ± 0.01	16.12 ± 0.05
2018-01-30	8149.3	+53.1	-	18.66 ± 0.02	17.40 ± 0.10	16.86 ± 0.10	16.19 ± 0.04
2018-02-02	8152.4	+56.2	-	18.57 ± 0.05	17.50 ± 0.05	16.94 ± 0.03	16.34 ± 0.04
2018-02-03	8153.3	+57.1	19.22 ± 0.21	18.61 ± 0.12	17.51 ± 0.07	16.94 ± 0.06	16.32 ± 0.07
2018-02-09	8159.4	+63.2	-	18.65 ± 0.02	17.63 ± 0.02	16.98 ± 0.02	16.41 ± 0.04
2018-02-13	8163.3	+67.1	19.08 ± 0.15	18.73 ± 0.03	17.69 ± 0.02	17.12 ± 0.03	16.50 ± 0.04
2018-02-16	8166.3	+70.1	19.14 ± 0.17	18.70 ± 0.07	17.76 ± 0.02	17.20 ± 0.03	16.57 ± 0.05
2018-02-20	8170.3	+74.1	-	18.77 ± 0.02	17.83 ± 0.01	17.28 ± 0.02	16.64 ± 0.04
2018-02-25	8175.2	+79.0	-	18.79 ± 0.11	17.90 ± 0.03	17.36 ± 0.03	16.72 ± 0.03
2018-03-07	8185.2	+89.0	-	18.96 ± 0.07	18.09 ± 0.02	17.53 ± 0.02	16.87 ± 0.05
2018-03-15	8193.3	+97.1	-	-	18.22 ± 0.01	17.69 ± 0.01	17.05 ± 0.02
2018-03-23	8201.4	+105.2	-	19.18 ± 0.02	18.35 ± 0.02	17.86 ± 0.02	17.19 ± 0.03
2018-03-30	8208.3	+112.1	-	-	18.47 ± 0.05	17.92 ± 0.04	17.30 ± 0.03
2018-04-02	8211.4	+115.2	-	19.28 ± 0.09	18.50 ± 0.05	18.02 ± 0.03	17.38 ± 0.05
2018-04-07	8216.3	+120.1	-	-	18.56 ± 0.02	17.99 ± 0.02	17.38 ± 0.02
2018-04-15	8224.3	+128.1	-	19.50 ± 0.02	18.71 ± 0.01	18.20 ± 0.01	17.60 ± 0.03
2018-04-21	8230.2	+134.0	-	19.64 ± 0.02	18.85 ± 0.03	18.30 ± 0.01	17.76 ± 0.02
2018-04-28	8237.4	+141.2	-	19.79 ± 0.17	18.98 ± 0.06	18.34 ± 0.04	17.86 ± 0.04
2018-05-01	8240.3	+144.1	-	-	19.03 ± 0.04	18.47 ± 0.03	17.88 ± 0.04
2018-05-30	8269.2	+173.0	-	-	-	18.83 ± 0.02	18.38 ± 0.04
2018-07-05	8305.2	+209.0	-	-	20.20 ± 0.03	19.41 ± 0.02	18.96 ± 0.03
2018-08-31	8362.1	+265.9	-	-	21.22 ± 0.14	20.28 ± 0.12	20.16 ± 0.15

\* With reference to the *B*-band maximum (JD 2458096.2).

lamp and spectrophotometric standards were obtained along with the SN for calibration purposes. The spectroscopic data reduction was carried out in a standard way using IRAF. After correcting the observed frames for bias and flat fields, one-dimensional spectra were extracted using the optimal extraction method. Wavelength calibration was done by applying the dispersion solutions obtained using arc lamp spectra. The night-sky emission lines were utilized to secure the wavelength calibration, and small shifts were applied wherever necessary. The spectrophotometric standard observed on the same night was used in obtaining the instrumental response curves for flux calibration of the spectra. For those nights where standard star observations were not possible, the response curves obtained during nearby nights were used. To construct a single flux calibrated spectrum, the spectrum in both the grisms (Gr#7, Gr#8) were combined. The spectra were then scaled with respect to the calibrated *UBVRI* fluxes to bring them to an absolute flux scale. Finally, the SN spectra were corrected for the host galaxy redshift of  $z = 0.006191$  (from NED).

### 3. PHOTOMETRIC EVOLUTION

#### 3.1. Estimation of explosion epoch and optical light curves

The last non-detection of SN 2017iro was reported (Wiggins 2017) on 2017 November 15.1 (JD 2458072.6) with a limiting magnitude of 19 mag. However, the SN was discovered on 2017 November 30.5 (JD 2458088.0). Since there is a large gap between the first detection and last non-detection various approaches were considered for estimating the explosion epoch. The explosion epoch was estimated by fitting a power law of the form  $L(t) = A \times (t - t_0)^{0.78}$  (Piro & Nakar 2013) to the pre-maximum phase of the LC. Here,  $L$  denotes the luminosity at time  $t$ ,  $A$  is a constant that defines rising rate, and  $t_0$  is the time of the explosion. The best fit value of  $t_0$  is computed as JD 2458077.1 (2017 November 21.1). While evaluating the explosion parameters of SN 2017iro (see Section 3.4), the model of Valenti et al. (2008) was best fitted for an explosion date of JD 2458084.0 (2017 November 26.5). Analytical function (Taddia et al. 2018) fitted to the LC (see Section 3.2) yielded an explosion epoch of JD 2458080.0 (2017 November 22.5). An average of the above values, i.e., JD 2458080.4  $\pm$  2.0 (2017 November 22.9), was adopted as the explosion epoch of SN 2017iro (see Table 4). Further, the typical rise times of Type Ib SNe in *R*-band and bolometric light curve are  $\sim$  22 d (Taddia et al. 2015) and  $\sim$  17 d (Lyman et al. 2016), respectively. The *R*-band and the bolometric peak of SN 2017iro occurred on JD 2458099.4 and JD 2458096.6, respectively (see Section 3.2). The mean explosion date estimated above is consistent with the rise time criteria.

The *UBVRI* light curves of SN 2017iro are shown in Fig. 2 (left panel). A well-sampled light curve covering

the pre-maximum to nebular phase was obtained using the photometric observation made on 40 epochs. In the right panel of Fig. 2, the *V*-band light curve of well-studied Type Ib SNe: iPTF13bvn (Srivastav et al. 2014; Kuncarayakti et al. 2015b), SN 2012au (Pandey et al. 2021), SN 2009jf (Sahu et al. 2011; Valenti et al. 2011), SN 2007Y (Stritzinger et al. 2009), and SN 1999dn (Benetti et al. 2011), having observations during pre-maximum and nebular phases are plotted along with SN 2017iro for comparison. The light curve evolution and estimation of related parameters are discussed in the following subsections.

#### 3.2. Light curve parameters

Various light curve parameters were obtained by fitting the light curves in different bands with an analytical function proposed by Taddia et al. (2018, see their section 3). This method is based on the empirical model suggested by Vacca & Leibundgut (1996) for thermonuclear events whose LCs are similar to that of SE-SNe. The epoch of maximum and the light curve parameters of SN 2017iro estimated from the LCs of different pass-bands are listed in Table 5 and are compared with other SE-SNe. A lag of  $\sim$ 5 d between *U* and *I*-band maximum is inferred for SN 2017iro. This duration is shorter in comparison to  $\sim$ 8 d for the slow-declining SN 2009jf (Sahu et al. 2011) and  $\sim$ 9 d for the fast-declining iPTF13bvn (Srivastav et al. 2014). The early appearance of maximum in bluer bands is a common behaviour of SE-SNe, and SN 2017iro follows this trend.

The luminosity decline rate parameter,  $\Delta m_{15}$  (difference in magnitude at peak and 15 d later), is handy in the context of Type Ia SNe, where it is found to be correlated with the peak luminosity. A smaller  $\Delta m_{15}$  value favours more luminous objects (Phillips 1993). Large data sets obtained from different surveys have provided an opportunity to investigate if such a correlation exists for SE-SNe. No direct correlation was found between the light curve decline rate parameter and luminosity by Drout et al. (2011) and Taddia et al. (2015). However, the sample study of a larger set of SE-SNe in Taddia et al. (2018) hinted towards the fact that luminous events tend to have broader light curves, i.e., a smaller value of  $\Delta m_{15}$ . In the following paragraph, we compared various light curve parameters of SN 2017iro with some well-studied Type Ib SNe.

The  $\Delta m_{15}$  values of SN 2017iro are 1.46, 0.77, 0.69 and 0.52 mag in *B*, *V*, *R* and *I* bands, respectively. These are similar to the values inferred for SN 2012au (Pandey et al. 2021, 1.60, 0.90, 0.70, and 0.43 mag, respectively). On the other hand, iPTF13bvn shows comparatively rapid evolution (1.82, 1.16, 1.22 and 0.90 mag, respectively, Srivastav et al. 2014) whereas SN 2009jf shows a relatively slower evolution (Sahu et al. 2011, 0.91, 0.50, 0.31, and 0.31 mag, respectively). The above can be inferred from the comparison of normalised *V*-band light curves shown in right panel of Fig. 2. The comparison

**Table 4.** Estimated explosion epoch of SN 2017iro using different methods (see Section 3.1).

Method adopted	Explosion epoch
Power law [ $L(t) = A \times (t - t_0)^{0.78}$ ] fit	JD 2458077.1 (2017 November 19.6)
Analytical fit (Taddia et al. 2018)	JD 2458080.0 (2017 November 22.5)
Toy model fit (Valenti et al. 2008)	JD 2458084.0 (2017 November 26.5)
Mean explosion epoch	JD 2458080.4 (2017 November 22.9)

**Table 5.** Light curve parameters of SN 2007iro (see Section 3.2).

Filter	Max epoch (JD)	$m_{\max}$ (mag)	$\Delta m_{15}$ (mag)	$\Delta m_{40}$ (mag)	Late time slope		$\Delta d_{0.25}$ (d)
					( $\sim 40 - 140$ d) (mag 100 d $^{-1}$ )	(>140d) (mag 100 d $^{-1}$ )	
<i>U</i>	$2458095.7 \pm 0.5$	$15.57 \pm 0.01$	$2.41 \pm 0.07$	$3.55 \pm 0.01$	—	—	$7.70 \pm 0.14$
<i>B</i>	$2458096.2 \pm 0.5$	$15.94 \pm 0.01$	$1.46 \pm 0.05$	$2.44 \pm 0.01$	1.27	—	$10.40 \pm 0.14$
<i>V</i>	$2458098.0 \pm 0.5$	$15.55 \pm 0.01$	$0.77 \pm 0.04$	$1.70 \pm 0.01$	1.73	1.80	$11.90 \pm 0.14$
<i>R</i>	$2458099.4 \pm 0.5$	$15.14 \pm 0.01$	$0.69 \pm 0.02$	$1.54 \pm 0.01$	1.57	1.52	$12.20 \pm 0.14$
<i>I</i>	$2458100.5 \pm 0.5$	$14.97 \pm 0.01$	$0.52 \pm 0.02$	$1.14 \pm 0.01$	1.75	1.90	$14.70 \pm 0.14$
Bolometric	$2458095.7 \pm 0.5$	$16.12 \pm 0.01$	$1.05 \pm 0.04$	$1.89 \pm 0.01$	1.65	—	$10.40 \pm 0.14$

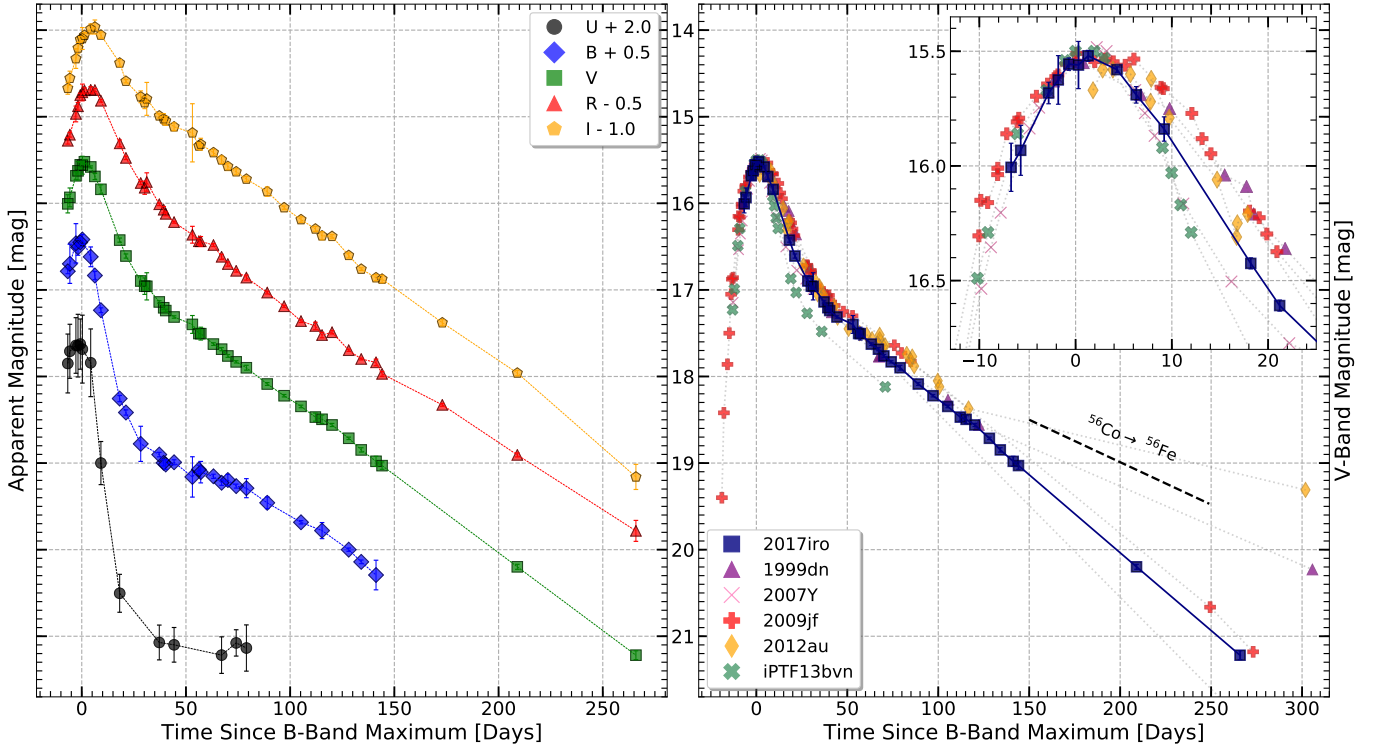


**Figure 2.** Left panel: The observed *UBVRI* light curves of SN 2017iro. For clarity, the light curves in different bands have been shifted vertically by the indicated amount. Right panel: The *V*-band magnitude of SN 2017iro is over-plotted with other Type Ib events i.e., iPTF13bvn, SN 2012au, SN 2009jf, SN 2007Y, and SN 1999dn (see Table 6 for references). The light curves of other events have been shifted arbitrarily to match the date of maximum and the peak magnitude to SN 2017iro. The evolution of light curves near the peak is also shown in the inset.

of early phase light curve indicates that the decline rate of SN 2017iro is intermediate between the fast declining SN 2007Y, iPTF13bvn and the slow declining SN 2009jf. The intermediate width of light curves of SN 2017iro could possibly indicate that ejecta mass of SN 2017iro lies in between the inferred ejecta mass of iPTF13bvn and SN 2009jf (see Section 5.3).

The decay in the magnitude from the peak to +40 d is denoted by the  $\Delta m_{40}$  parameter by Taddia et al. (2018).  $\Delta m_{40}$  was found to be in the range of 1.5 to 1.7 mag (in  $r$ -band) for their sample of SE-SNe. SN 2017iro lies towards the lower end (1.54 mag in  $R$ -band) of the observed range, indicating a relatively faster evolution for a SE-SN. The late phase ( $> 40$  d) light curve decay rate of SN 2017iro is also computed in all bands (see Table 5). The decay rates between  $\sim +40$  to  $\sim +140$  d are 1.27, 1.73, 1.57 and 1.75 mag  $100 \text{ d}^{-1}$  (in  $B$ ,  $V$ ,  $R$  and  $I$  bands, respectively) and beyond  $\sim 140$  d is 1.80, 1.52 and 1.90 mag  $100 \text{ d}^{-1}$  (in  $V$ ,  $R$  and  $I$  bands, respectively). It is to be noted that usually, SE-SNe display faster decline than Type II events during the late phases. Such features are indicative of higher  $\gamma$ -rays escape. The implications of the fast declining nature of SN 2017iro is discussed in Section 5.1.

The  $V$ -band absolute magnitude ( $M_V$ ) of SE-SNe is known to display a wide range between  $\sim -16.5$  to  $\sim -19.5$  mag (Richardson et al. 2006; Drout et al. 2011; Taddia et al. 2018). To estimate the  $M_V$  of SN 2017iro, we adopted distance of the host galaxy NGC 5480 as  $30.8 \pm 2.2$  Mpc (corrected for Virgo infall only) and the corresponding distance modulus  $32.44 \pm 0.15$  mag (for an  $H_0 = 73 \text{ km s}^{-1} \text{ Mpc}^{-1}$ ). The adopted distance is consistent with the distance estimate of 30.73 Mpc using Tully-Fisher relation (Theureau et al. 2007). After applying a correction for the reddening  $E(B-V) = 0.28$  mag (see Section 3.3), the  $M_V$  of SN 2017iro is derived as  $-17.76 \pm 0.15$  mag. This indicates that SN 2017iro is fainter than SN 2007uy, SN 2009jf and SN 2012au but brighter than SN 2007Y and iPTF13bvn.

### 3.3. Reddening and colour evolution

The estimate of reddening suffered by SN is crucial as it affects the explosion parameters which are derived using the observables. The reddening due to ISM in the Milky Way along the line of sight (LOS) of the SN can be inferred using the all-sky dust extinction map (e.g. Schlafly & Finkbeiner 2011; Schlafly et al. 2016). The determination of reddening within the host galaxy is a challenging task. In general, the sites of SE-SNe, are associated with star-forming regions (e.g. Anderson et al. 2012; Eldridge et al. 2013) and may suffer a considerable amount of reddening. Several photometric and spectroscopic techniques have been proposed to determine the reddening within the host galaxy but with caveats.

The Galactic reddening along the LOS of SN 2017iro as derived from the all-sky dust extinction map (Schlafly & Finkbeiner 2011) is  $E(B-V) = 0.016 \pm 0.001$  mag.

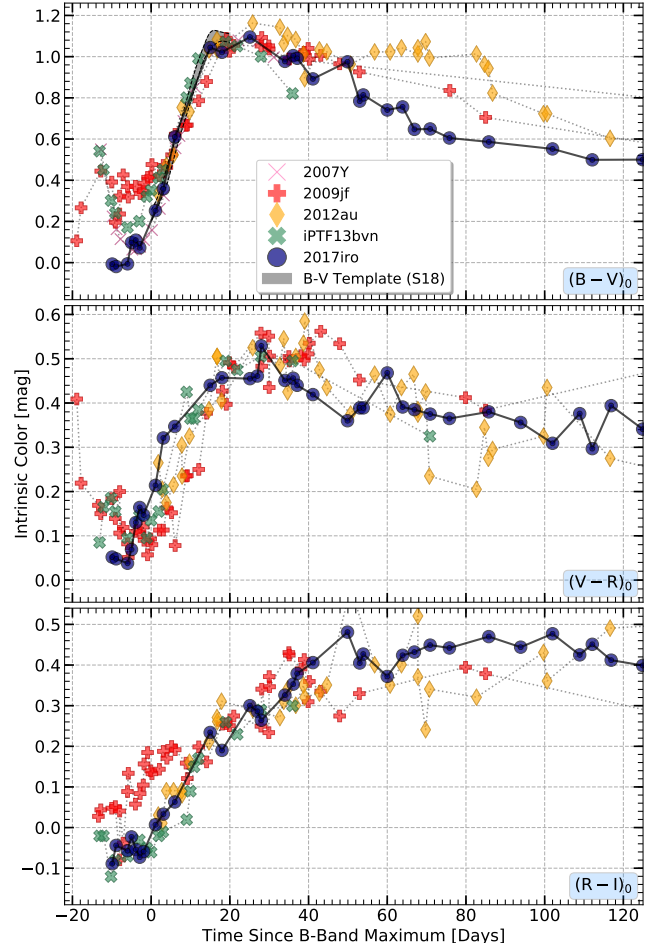


**Figure 3.** Colour evolution of SN 2017iro, plotted along with iPTF13bvn, SN 2012au, SN 2009jf, SN 2007uy and SN 2007Y. Both the MW and the host galaxy extinction corrections have been applied for each SN. The  $B-V$  colour templates from Stritzinger et al. (2018) are over-plotted in the top panel for comparison. The bibliographic sources are the same as mentioned in the text (Section 3).

The equivalent width (EW) of Na I D absorption lines is considered as a good tracer of reddening within the host-galaxy (Barbon et al. 1990; Turatto et al. 2003; Poznanski et al. 2012) but with caveats (Poznanski et al. 2011; Phillips et al. 2013). To estimate the EW of Na I D, we stacked the low-resolution spectra of SN 2017iro obtained near the maximum light. A reasonably strong Na I D absorption feature is seen at the redshift of the host galaxy with an  $\text{EW} = 1.34 \pm 0.10 \text{ \AA}$ . An average value of  $E(B-V)_{\text{host}}$ , computed from the relation of Barbon et al. (1990) and Turatto et al. (2003) is  $0.27 \pm 0.04$  mag. For further analysis we adopt a total extinction  $E(B-V)_{\text{MW}+\text{host}} = 0.28 \pm 0.04$  mag (Milky Way + host) and Cardelli et al. (1989) extinction law with ratio of selective to total extinction  $R_V = 3.1$ .

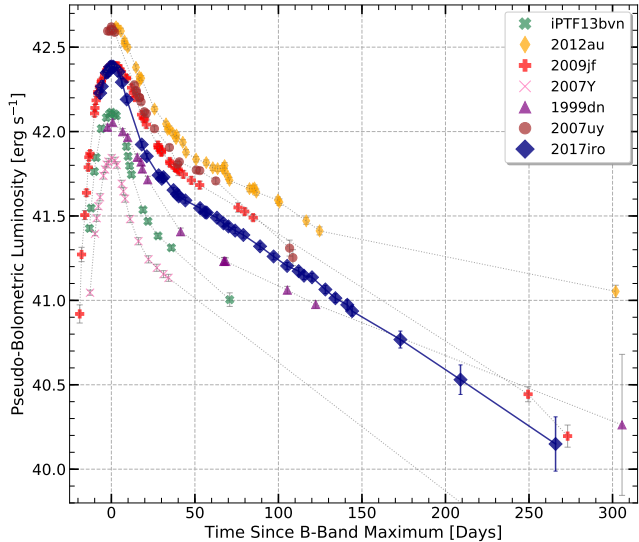


**Figure 4.** The pseudo-bolometric light curve of SN 2017iro (connected with a bold line) compared with other similar Type Ib events (iPTF13bvn, SN 2012au, SN 2009jf, SN 2007uy, SN 2007Y and SN 1999dn). The pseudo-bolometric light curves were obtained using SUPERBOL.

**Table 6.** Sample of Type Ib SNe used in this study.

Name	$E(B - V)_{tot}$ (mag)	Distance (Mpc)	References
SN 1999dn	0.10	38.90	1
SN 2007Y	0.11	19.31	2
SN 2007uy	0.63	29.50	3
SN 2009jf	0.11	34.25	4, 5
SN 2012au	0.06	23.50	6, 7
iPTF13bvn	0.22	22.49	8, 9

References: <sup>1</sup>(Benetti et al. 2011), <sup>2</sup>(Stritzinger et al. 2009), <sup>3</sup>(Roy et al. 2013), <sup>4</sup>(Sahu et al. 2011), <sup>5</sup>(Valenti et al. 2011), <sup>6</sup>(Milisavljevic et al. 2013a), <sup>7</sup>(Takaki et al. 2013), <sup>8</sup>(Srivastav et al. 2014), <sup>9</sup>(Kuncarayakti et al. 2015b).

In Fig. 3, the  $B - V$ ,  $V - R$ , and  $R - I$  colours of SN 2017iro are compared with other well-studied Type Ib events (see Table 6 for details and references). It is seen that the overall shape of colour evolution for each colour is similar (also see Stritzinger et al. 2018). Up to  $\sim +20$  d, the  $B - V$  colour evolves faster than the  $V - R$  and  $R - I$  colours. During the late phase ( $> 20$  d), the colour evolution is almost flat.

### 3.4. Quasi-bolometric light curve

The quasi-bolometric light curve of SN 2017iro was constructed using the latest version of Python-based code *SuperBol* (Nicholl 2018). The  $UBVRI$  magnitudes after correcting for the total extinction  $E(B - V) = 0.28$  mag, and adopted distance to NGC 5480 were given as input parameters. The  $U$  and  $B$  band magnitudes were extrapolated by assuming a constant colour during the late phases. The flux integration was performed only over the optical wavelengths. The resultant

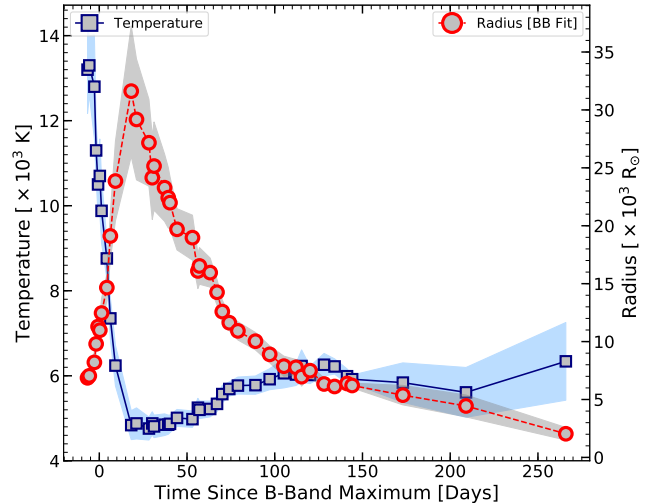


**Figure 5.** The blackbody temperature and radius evolution of SN 2017iro. These parameters were derived from the photometric data using SUPERBOL. The shaded regions indicate 1- $\sigma$  uncertainties.

quasi-bolometric light curve of SN 2017iro along with well studied Type Ib events (estimated similarly) are shown in Fig. 4. Furthermore, the black body fit parameters (temperature and radius) which is a default outcome of the code is also plotted in Fig. 5.

We fitted Taddia et al. (2018) equation to the quasi-bolometric light curve of SN 2017iro and estimated parameters listed in Table 5. The light curve peaked at JD 2458095.7 with  $\log_{10} L = 42.39 \pm 0.09$  erg s<sup>-1</sup>. The  $\Delta m_{15_{bol}}$  value of SN 2017iro is 1.05 mag, which is higher than that of SN 2009jf (0.60 mag) but is comparable to SN 2007Y (0.80 mag). The decay rates after +40 d of SN 2017iro (0.016 mag d<sup>-1</sup>) and SN 2009jf (0.014 mag d<sup>-1</sup>) are similar implying relatively faster evolution than the cobalt decay rate ( $\sim 0.01$  mag d<sup>-1</sup>, see also Section 5.1). This decay rate is consistent with the range 0.014–0.018 mag d<sup>-1</sup> seen in Type Ib events (Taddia et al. 2018).

## 4. SPECTROSCOPIC EVOLUTION

The early (photospheric phase) spectra are useful to examine the outermost regions of the expanding ejecta. For example, the presence/absence of residual hydrogen and/or helium during the pre-explosion stellar evolution can be explored with the early phase spectra. In the nebular phase, because of expansion, the ejecta becomes optically thin, and hence spectra during this phase provide essential information about the inner layers of the ejecta.

In this section, the spectral evolution of SN 2017iro covering pre-maximum to nebular phase is presented. The densely sampled spectroscopic data provided an opportunity to compare important spectral features with other well-studied events. All spectra were corrected



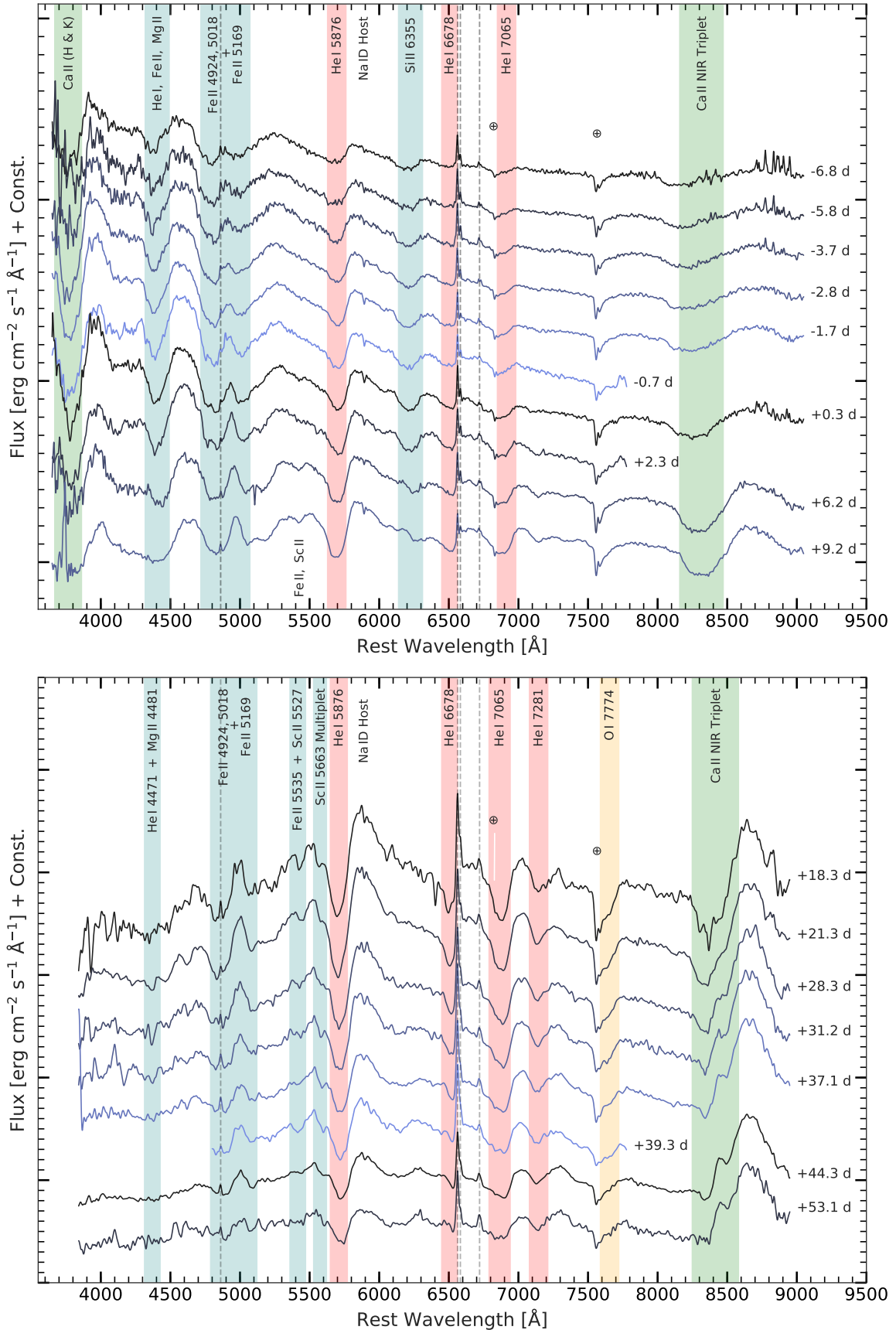


**Figure 6.** Pre-maximum along with early post-maximum ( $-7$  to  $+9$  d) and late post-maximum ( $+18$  to  $+53$  d) phases spectral evolution of SN 2017iro are shown in the top and bottom panels, respectively. Prominent spectral lines are marked. The labelled phases are with respect to the  $B$ -band maximum (JD 2458096.2). The spectra have been corrected for redshift and reddening. Features arising from the host are marked with dashed vertical lines. Major telluric bands are shown with a circled plus symbol. The spectra shown in Figures 6, 8 and 9 are available as data behind the figure.

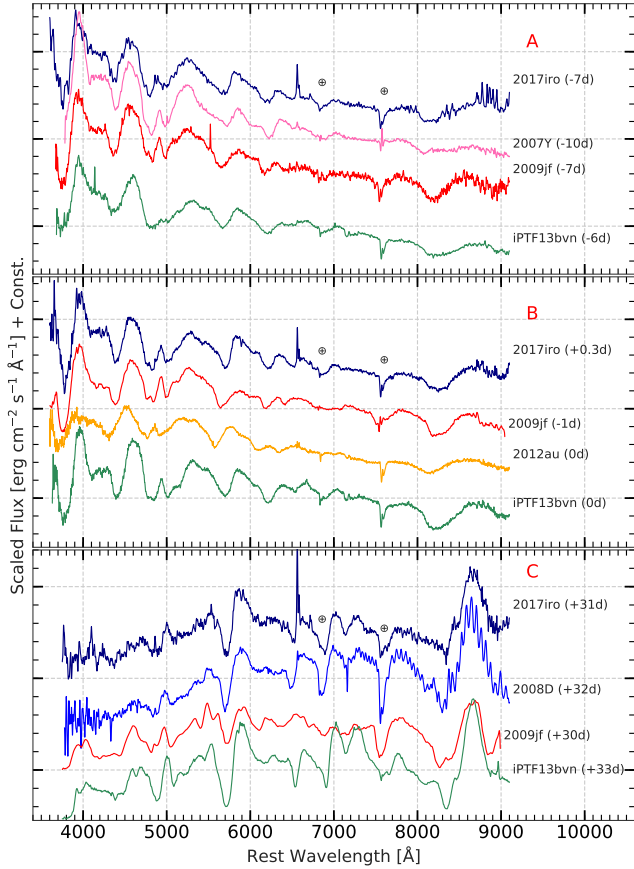


**Figure 7.** SN 2017iro spectral evolution compared with other Type Ib events (iPTF13bvn, SN 2012au, SN 2009jf, SN 2008D and SN 2007uy) at similar epochs. Panels A, B and C represent the pre-maximum, near-maximum and post-maximum spectra, respectively. Telluric lines are shown with circled plus symbols.

for the heliocentric velocity of  $1856 \text{ km s}^{-1}$  of the host galaxy (NGC 5480). The evolution of spectroscopic features is discussed in the following sections.

#### 4.1. Pre-maximum and early post-maximum phase

The spectral evolution in the pre-maximum and around maximum phase is shown in Fig. 6 (top panel). During early phase (i.e. pre-maximum), spectroscopy of SN 2017iro was done almost every night. The first spectrum at  $\sim -7$  d clearly shows the broad absorption feature of He I 5876 Å line, and weak signatures of other He I lines. He I 6678 Å is blended with narrow H $\alpha$  line from the host galaxy, whereas the He I 7065 Å feature lies at the edge of the telluric absorption band at 6870 Å. Other narrow lines (H $\beta$  4861 Å, [N II] 6584 Å and [S II] 6717, 6731 Å) originating from the underlying H II region are also clearly visible. In the extreme blue region of the observed spectra, well developed Ca II H & K lines (3934 and 3968 Å) are seen. The spectrum also shows features of Fe II triplet (4924, 5018 and 5169 Å), Si II

6355 Å and a weak absorption due to Ca II NIR triplet (8498, 8542 and 8662 Å).

In the pre-maximum spectral evolution, the region between 4000 to 4300 Å appears flat, possibly due to the blending of metal lines in the spectra. The absorption around 4400 Å is possibly a blend of He I, Fe II and Mg II. As the SN evolves towards the maximum, the lines due to He I, Fe II, and Si II become more prominent. In the early post-maximum spectra, the Si II 6355 Å feature starts weakening and vanishes in the spectra obtained on +18 d (cf. Fig. 6, bottom panel). A feature around 5500 Å begins to develop in the spectrum of  $\sim +6$  d, which is likely a blend of Fe II 5535 Å and Sc II 5527 Å lines. The Na I D lines from the host galaxy are seen as a narrow absorption in the spectra.

The spectra of SN 2017iro during the pre-maximum (Fig. 7, Panel: A) and close to maximum phase (Fig. 7, Panel: B) are compared with the spectra of few other well-studied Type Ib SNe SN 2009jf (Sahu et al. 2011), iPTF13bvn (Srivastav et al. 2014; Kuncarayakti et al. 2015b), SN 2007Y (Stritzinger et al. 2009), SN 2008D (Modjaz et al. 2009b) and SN 2012au (Pandey et al. 2021) around similar epochs. A good similarity can be noticed in the spectrum of SN 2017iro obtained at  $-7$  d and near maximum with those of SN 2009jf and iPTF13bvn. Except for iPTF13bvn, the Fe II line near 5000 Å is found to be prominent in other SNe used in comparison (cf. panel: A in Fig. 7). However, in SN 2017iro, the Fe II line appears to be contaminated by narrow H $\beta$  line from the underlying H II region. The spectrum of SN 2012au is shifted blue-wards (cf. panel: B in Fig. 7) due to its higher expansion velocity (Milisavljevic et al. 2013a; Takaki et al. 2013).

#### 4.2. Late post-maximum and early nebular phase

The spectral evolution during +18 to +53 d is displayed in the bottom panel of Fig. 6. The continuum becomes redder during this phase, and the Ca II H & K lines disappear, and other metallic lines appear in this part of the spectrum. However, the region below 4500 Å in our spectrum, is noisy, so lines could not be identified. The He I lines are initially prominent, but beyond +45 d, they weaken. In the blue wing of He I 5876 Å line, lines due to Sc II start emerging. The Fe II lines around 5000 Å also start blending. The Ca II NIR triplet gradually transformed into emission dominated. Beyond +40 d, when the light curve enters into the exponential decline, the forbidden lines [O I] 6300, 6364 Å and [Ca II] 7291, 7324 Å start appearing.

From the light curve, it is clear that the supernova entered into the linear decline phase beyond 50 d after the explosion, which indicates a transition from the photospheric phase to the nebular phase. The emergence of nebular lines, especially the forbidden lines of [O I] 6300, 6364 Å and [Ca II] 7291, 7324 Å also signifies the transition to the nebular phase. The spectrum taken during +67 to +112 d is displayed in Fig. 8. During this phase,

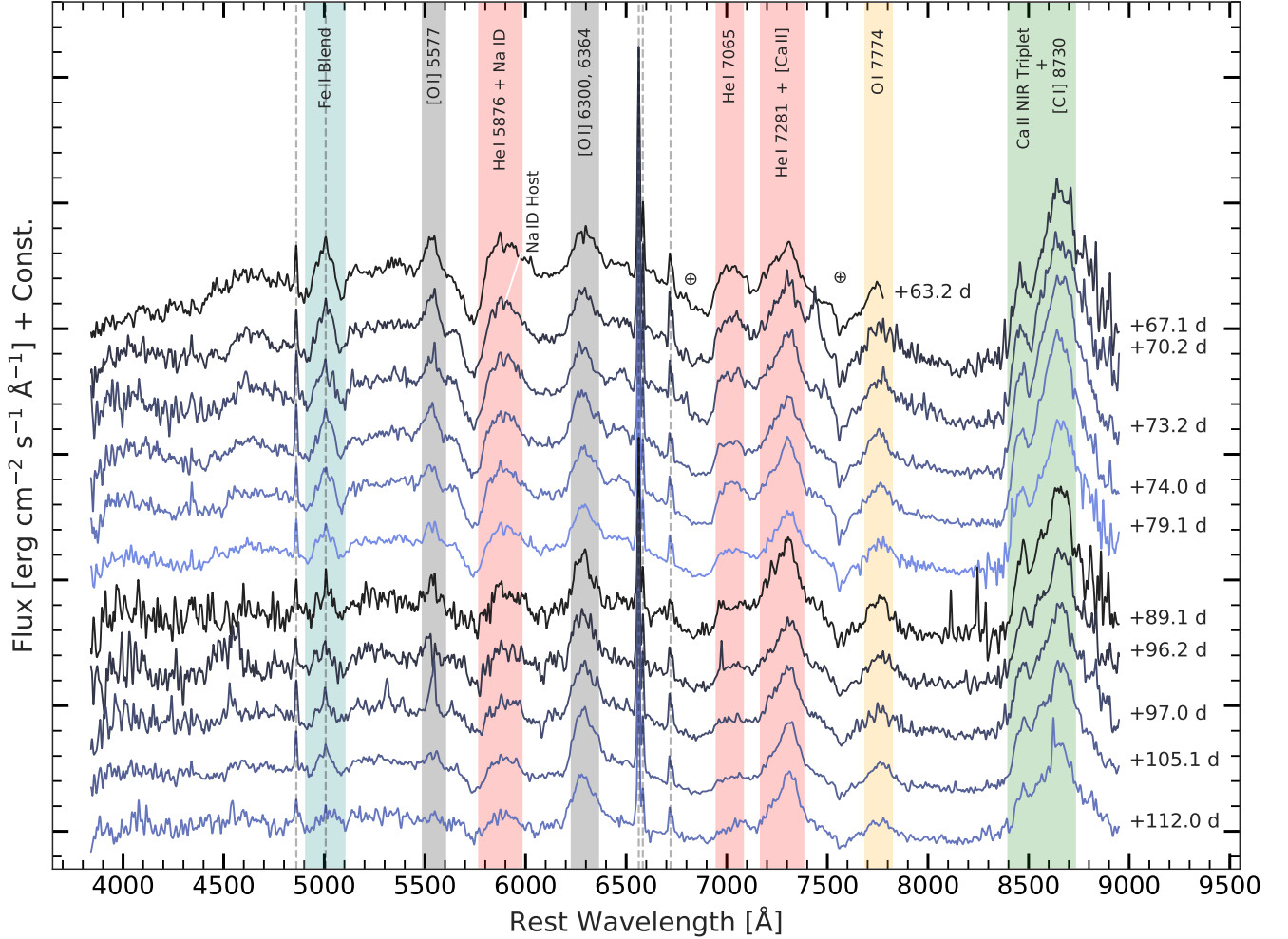


**Figure 8.** Late post-maximum and early nebular phase ( $\sim +67$  to  $+112$  d) spectral evolution of SN 2017iro. Prominent spectral lines are also marked. Other descriptions are similar as mentioned in Fig. 6. The spectra shown in Figures 6, 8 and 9 are available as data behind the figure.

the spectra are slowly getting dominated by the forbidden emission lines. The nebular line [O I] 5577 Å is also seen along with O I 7774 Å line, which is probably powered by an oxygen recombination cascade. The Ca II NIR triplet is dominated by the emission component and possibly blended with the [C I] 8730 Å line. The spectrum obtained on  $+112$  d still shows the presence of continuum and is not fully nebular. In Fig. 7 (panel: C), the spectra near a month after the maximum light is compared. The  $\sim +31$  d spectrum of SN 2017iro is similar to the spectrum of iPTF13bvn and SN 2008D. Also, He I 6678, 7065 Å lines in SN 2009jf are weaker as compared to other SNe. It is also worth mentioning that between 4000–5000 Å SN 2017iro and SN 2008D exhibit comparatively flat structures however, iPTF13bvn and SN2009jf have strong features in this wavelength range.

#### 4.3. Nebular phase

The spectra taken during  $+134$  to  $+209$  d is presented in Fig. 9. The spectra are dominated by the forbidden emission lines of [O I] and [Ca II], narrow lines from the nearby H II region are also clearly seen. The [O I] 5577 Å which was fairly strong in the early nebular phase (before  $\sim 100$  d), faded after that and almost vanished in the nebular spectra. The semi-forbidden line Mg I] 4571 Å is found to be always weak in the spectra of SN 2017iro. The emission component of the Ca II NIR triplet, which was stronger till  $\sim 120$  d starts weakening, and by  $\sim 176$  d it merges with the almost flat continuum. The forbidden [O I] and [Ca II] lines show complex profile.

In Fig. 10, the nebular phase spectrum of SN 2017iro at  $+209$  d is compared with those of other type Ib events, obtained at similar epoch. The emission features of semi-forbidden Mg I] 4571 Å, forbidden [O I] 6300, 6364 Å, and [Ca II] 7291, 7324 Å are prominently visible in these SNe. It is interesting to note

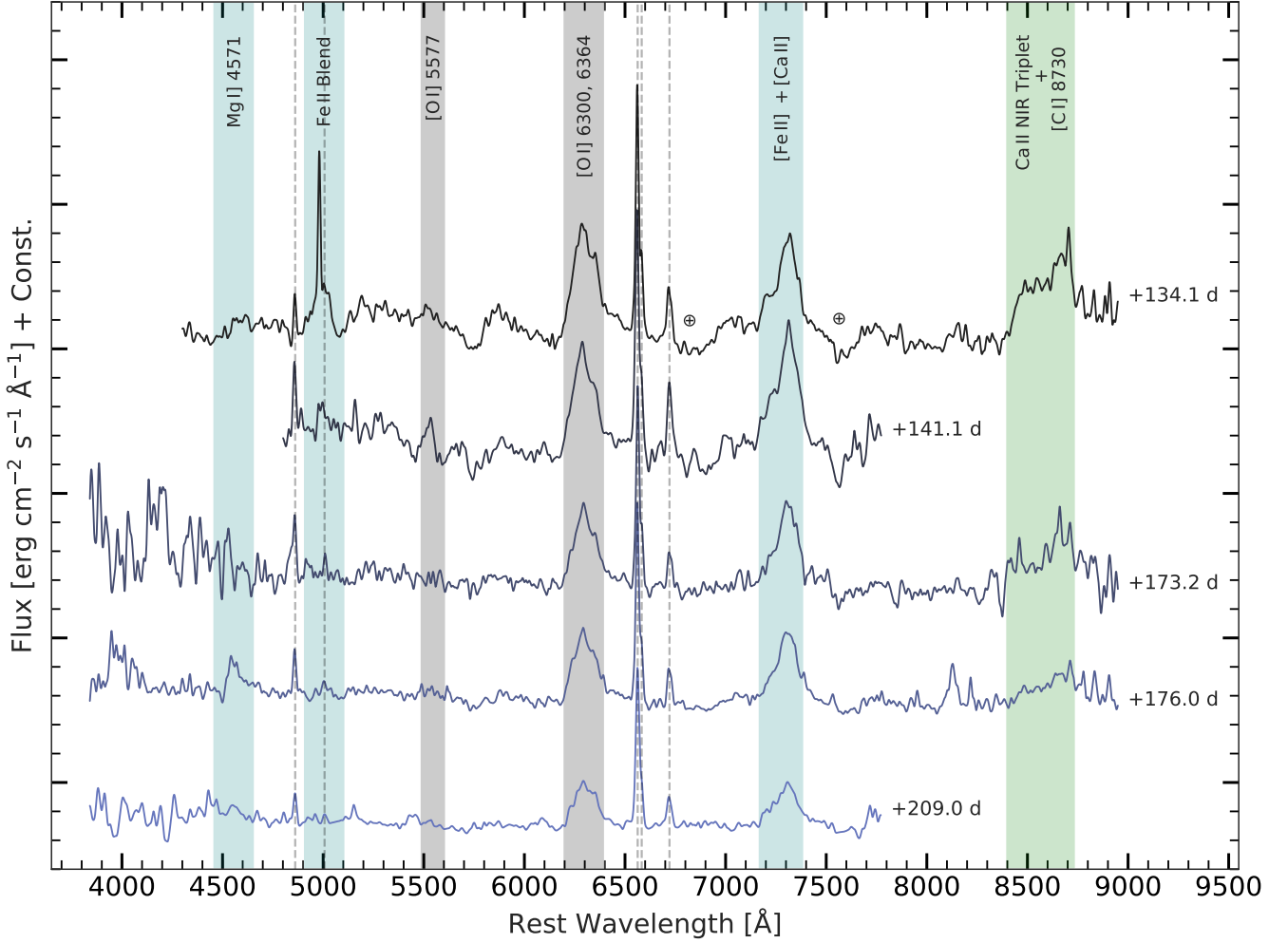


**Figure 9.** Nebular phase ( $\sim+134$  to  $+209$  d) spectra of SN 2017iro. Various nebular emission lines are shown. The dashed vertical lines indicate the features arising from the host and the telluric bands are shown with a circled plus symbol (for other descriptions, see Fig. 6). The spectra shown in Figures 6, 8 and 9 are available as data behind the figure.

that in SN 2017iro, the strength of [O I] and [Ca II] lines are similar whereas, in SN 2009jf, SN 2012au and Master OT J120451.50+265946.6 (MOT) the [O I] line is stronger than the [Ca II] line. In SN 2017iro, the Mg I] is comparatively very weak than other SNe. The ratio of Mg I] to [O I] lines in SN 2017iro is estimated as  $\sim 0.15$  which is similar to MOT ( $\sim 0.3$ , Singh et al. 2019) but lesser than iPTF13bvn ( $\sim 0.85$ , Kuncarayakti et al. 2015b).

Amongst the nebular forbidden emission lines, the Mg I] line lies in the bluer and crowded region of the spectra, where generally signal is poor. Furthermore, Ca is a trace element and its distribution is not necessarily representative of the bulk of the ejecta. Hence, the [O I] doublet which emerges in relatively clear region, is generally used as the tracer of the explosion geometry (Mazzali et al. 2005; Maeda et al. 2008a; Modjaz et al. 2008a; Taubenberger et al. 2009; Milisavljevic et al. 2010). From the Fig. 10, similarity between nebu-

lar spectrum of SN 2009jf and SN 2017iro is evident with [O I] line profile being asymmetric and multi-peaked in both the objects. However, asymmetry in [O I] line profile of SN 2017iro is weaker as compared to SN 2009jf with the peaked component of [O I] line centered at rest wavelength. The asymmetric and multi-component [O I] profile, seen in the nebular spectra, can be reproduced with a complex ejecta geometry of an aspherical explosion (Mazzali et al. 2005; Maeda et al. 2007a). The observed features in the asymmetric [O I] line profile in SN 2017iro, could be explained with a high density core of the ejecta (Taubenberger et al. 2009; Maeda et al. 2008a).

The gas-phase oxygen abundance in the vicinity of supernova location is estimated using the relation of Pettini & Pagel (2004). N2 and the O3N2 indices were computed from the last spectrum obtained on  $\sim 209$  d. The average value of oxygen abundance  $12 + \log(\text{O}/\text{H})$  (estimated using O3N2 and N2 indices) for the super-

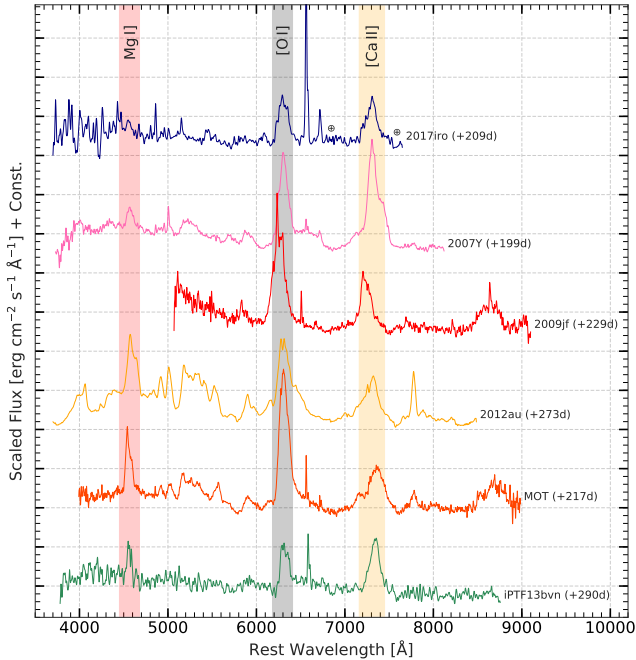


**Figure 10.** Comparison of nebular phase spectral features of SN 2017iro with other well studied Type Ib events. The SN references are same as described in Section 4.1 in addition to Master OT J120451.50+265946.6 (MOT, Singh et al. 2019).

nova region is found to be  $8.64 \pm 0.2$  which is remarkably similar to iPTF13bvn ( $8.63$ , Kuncarayakti et al. 2015b). In a recent study under the CALIFA (Sánchez et al. 2012) survey program, Galbany et al. (2016) used wide-field integral field spectroscopy to compute the global metallicity of NGC 5480 and metallicity at the location of SN 1988L. The estimated values are  $8.58$  and  $8.55$  for the local and global, respectively. This shows that our estimate of the oxygen abundance is in fairly good agreement with the previous study, and is close to the solar value of  $12 + \log(\text{O}/\text{H}) = 8.69 \pm 0.05$  (Asplund et al. 2009). Further, the computed metallicity close to the SN location is similar to the estimates of Modjaz et al. (2011,  $8.49 \pm 0.19$ ) and Sanders et al. (2012,  $8.48 \pm 0.16$ ), made at the location of other SNe Ib.

#### 4.4. Line velocities

The velocities of lines Fe II 5169 Å, He I 5876 Å, He I 6678 Å and Si II 6355 Å were estimated by fitting Gaussian profile to the respective absorption trough after correcting the spectra for the redshift of host galaxy of SN 2017iro. The estimated line velocities of SN 2017iro along with SNe 2007Y, 2008D, 2009jf, 2012au, and iPTF13bvn collected from the literature are plotted in Fig. 11. In case of SN 2017iro, the He I 5876 Å velocity is  $\sim 11500 \text{ km s}^{-1}$  in the beginning and declined to  $\sim 9000 \text{ km s}^{-1}$  near maximum. In the post-maximum phase, it evolves slowly and becomes flat ( $\sim 7000 \text{ km s}^{-1}$ ) after +70 d. All the SNe (except SN 2007Y), used in

the comparison, show a steep decline in the He I 5876 Å line velocity during the pre-maximum phase. The post-maximum evolution of He I shows a modest increase of  $\sim 900 \text{ km s}^{-1}$  giving rise to a bump like feature in the velocity evolution. A similar feature can also be seen in SN 2009jf, iPTF13bvn, and SN 2008D during maximum to  $\sim +20$  d. The origin of this feature needs to be explored. The evolution of He I 5876 Å line velocity beyond  $\sim +25$  d, is similar in SN 2017iro, iPTF13bvn, and SN 2009jf but lower than SN 2012au. In homologous expanding SNe ejecta, it is difficult to accurately determine the photospheric velocity from the observed spectral features as none measurable feature of the spectra is connected directly to photospheric velocity (Takáts & Vinkó 2012). However, the prominent absorption features produced due to Fe II 5169 Å can be used as a good tracer of SN photospheric velocity as it is a less optically thick line compared to several others lines (Dessart & Hillier 2005). The Fe II line velocity of SN 2017iro is compared in the middle panel of Fig. 11. The ejecta velocity measured using Fe II line of all the SNe shows a steep decline till  $\sim +25$  d and flattens thereafter. The Fe II line velocity of SN 2017iro near-maximum is comparable to SN 2007Y, SN 2009jf, and iPTF13bvn, but slower than SN 2008D and SN 2012au. In the later phase ( $> +25$  d), the Fe II line velocity of SN 2017iro is in between SN 2009jf and SN 2007Y. The Fe II velocity around maximum light ( $\sim 9000 \pm 800 \text{ km s}^{-1}$ ) is used to estimate the explosion energy of SN 2017iro (see Section 5.3).

## 5. DISCUSSION

The observed fraction of Type Ib SNe is low, they are rare objects (Li et al. 2011b; Graur et al. 2017a,b; Shivvers et al. 2019). There are only a handful events for which studies covering both photospheric and nebular phases are available. A detailed investigation of SN 2017iro, hence is a good addition to this sample as it fills the gap between fast declining (e.g. SN 2007Y, iPTF13bvn) and slow declining (e.g. SN 2009jf) objects (see Section 3.2). Here, we discuss the nature of SN 2017iro based on some significant light curve and spectral features, constrain its progenitor mass, and also estimate the explosion parameters.

### 5.1. Late phase light curve heterogeneity

The light curve of SE-SNe follows a linear decline with the onset of the nebular phase (usually  $> 100$  days after the explosion). This is a consequence of energy injection from the radioactive decay of  $^{56}\text{Co} \rightarrow ^{56}\text{Fe}$ . The efficiency of  $\gamma$ -ray trapping within the ejecta affects the decay rate. In general, it is found that the late phase light curve of SE-SNe declines faster than the expected decay rate of  $0.98 \text{ mag (100 d)}^{-1}$  from  $^{56}\text{Co} \rightarrow ^{56}\text{Fe}$  transition. This is primarily due to the lower opacity of the ejecta for the  $\gamma$ -rays (i.e., incomplete trapping). Therefore, the light curve decay rate during the nebular

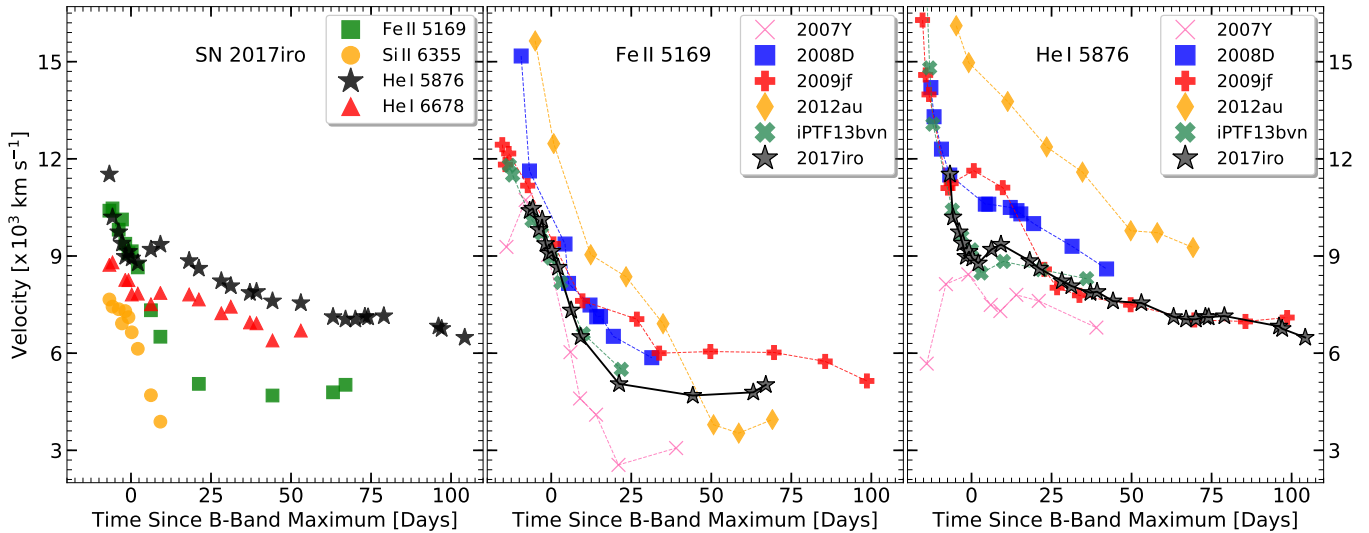


**Figure 11.** Evolution of the velocity of different spectral lines observed in SN 2017iro. Error in these estimates was never below  $800 \text{ km s}^{-1}$ . The line velocities of different SNe (SN 2007Y, 2008D, 2009jf, 2012au and iPTF13bvn) are also compared.

phase can be used to infer the ratio of explosion energy, and mass of the ejecta. The late phase (beyond 140 d) decline rate of SN 2017iro is estimated in different bands and are listed in Table 5. The light curves are found to decline significantly faster than  $0.98 \text{ mag (100 d)}^{-1}$ .

An investigation of the late time light curve of SE-SNe by Wheeler, Johnson, & Clocchiatti (2015) revealed the diverse nature of their evolution, indicating dispersion in the ejecta masses and kinetic energies. Our comparison of the late-time decay rate of well studied Type Ib SNe (cf. Fig. 2: right panel) indicates that there exist two groups of events. SN 1999dn and SN 2012au fall under the first category in which the late phase decline rate is significantly slower than the  $^{56}\text{Co} \rightarrow ^{56}\text{Fe}$  decay rate. The slower light curve decline rate indicates the need for an additional source of energy which could be interaction of the ejecta with the circumstellar material (CSM), a magnetar or presence of light echo. Wheeler et al. (2015) suggested the presence of CSM in SN 1999dn. The presence of smoothly distributed CSM around SN 2012au was inferred from its detection in radio wavebands (Kamble et al. 2014). However, very late nebular spectrum of SN 2012au, obtained  $\sim 6.2$  years after the explosion, indicated magnetar/pulsar wind nebulae as the most probable energy source (Milisavljevic et al. 2018). In the second group of SE-SNe, the light curve decline rate is faster than the expected decline rate of  $^{56}\text{Co} \rightarrow ^{56}\text{Fe}$ . The faster decline rate could be due to incomplete trapping of  $\gamma$ -rays produced via  $^{56}\text{Co} \rightarrow ^{56}\text{Fe}$  decay, in the SN ejecta. The late-time decay rate of SN 2017iro indicates it falls in this category and is similar to that of SN 2009jf, SN 2007Y and iPTF13bvn. It is worth mentioning that during the late nebular phase, an increasing fraction of photons emitted at IR wavelength may also steepen the decline rate in optical bands.

## 5.2. $^{56}\text{Ni}$ mixing

The lines of He I, the identifying features of Type Ib SNe, are seen at a velocity of  $\sim 11500 \text{ km s}^{-1}$  in the first spectrum ( $\sim -7 \text{ d}$ ) of SN 2017iro (cf. Fig. 11). The origin of these lines require non-thermal excitation and ionization (Lucy 1991; Swartz 1991). The accelerated electrons responsible for the non-thermal excitation are regulated by the  $\gamma$ -rays produced in the radioactive decay of newly synthesized  $^{56}\text{Ni}$  (Harkness et al. 1987). It is shown that the mere presence of an appreciable amount of helium in the progenitor would not lead to the presence of helium lines in the spectra (Dessart et al. 2012). To excite He I at high velocities,  $\gamma$ -rays need to be in the proximity of the helium layer, either due to the leakage of  $\gamma$ -rays through the inner ejecta or by substantial mixing of  $^{56}\text{Ni}$  up to the outer ejecta.

Mixing may arise due to various reasons such as large-scale asymmetric explosion jets and asymmetry of the propagating shock etc. (see, Maund et al. 2009; Couch et al. 2011; Dessart et al. 2012, and references therein). The effect of  $^{56}\text{Ni}$  mixing on the light curves and spectra of SE-SNe have been investigated in detail by several authors. Theoretical studies (Shigeyama et al. 1990; Hachisu et al. 1991) argued that  $^{56}\text{Ni}$  mixing within the helium layer might depend on the progenitor composition. The degree of  $^{56}\text{Ni}$  mixing may also significantly influence the overall light curve shape (including the post-maximum phase) and the efficient formation of He I spectral lines (Ensmann & Woosley 1988; Woosley & Eastman 1997; Shigeyama et al. 1990; Cano et al. 2014; Dessart et al. 2015, 2016; Taddia et al. 2018).

The early time colour evolution of Type Ib/c SNe can also be used as a diagnostic for the  $^{56}\text{Ni}$  distribution in the ejecta. It is shown that in the case of strong mixing, the colour curves of Type Ib/c SNe monotonically red-

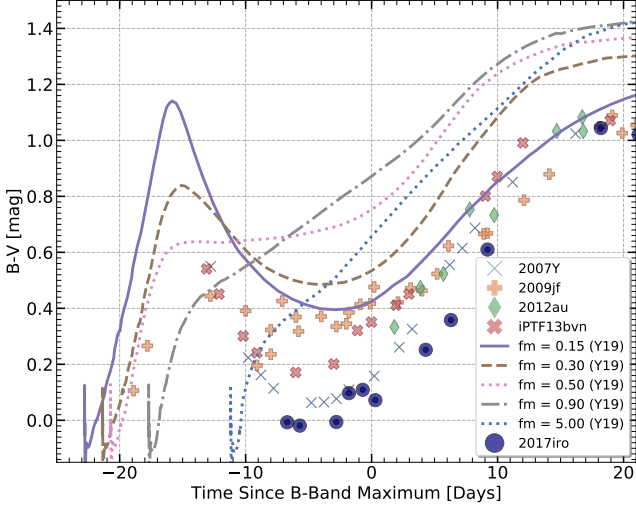


**Figure 12.** The  $B - V$  colour evolution of SN 2017iro compared with the synthetic colour curves of SN Ib models by Yoon et al. (2019). The five bold curves indicate varying degrees of  $^{56}\text{Ni}$  mixing ( $f_m$ ) as shown in the legend (Y19). An increasing value of  $f_m$  implying a stronger  $^{56}\text{Ni}$  mixing (for more details, see Yoon et al. 2019).

den during the photospheric phase, because of continuous and progressive effects of  $^{56}\text{Ni}$  heating. Whereas, in the case of weak to moderate mixing, the colour evolution does not show monotonic behaviour due to delayed heating from  $^{56}\text{Ni}$  (Yoon et al. 2019, and references therein). The early phase  $B - V$  colours of different Ib events along with  $^{56}\text{Ni}$  mixing models (Yoon et al. 2019) are plotted in Fig. 12. The colour evolution of SN 2007Y, SN 2009jf, and iPTF13bvn follow a non-monotonic trend which is interpreted in the framework of weak to moderate mixing of  $^{56}\text{Ni}$  in the ejecta. However, the non-availability of sufficiently early phase data points for SN 2017iro prevents us from arriving at any firm conclusion on the role of mixing.

### 5.3. Physical parameters of explosion

The peak of the light curve and its shape in SE-SNe are mainly regulated by the synthesized radioactive  $^{56}\text{Ni}$ , kinetic energy ( $E_k$ ) and ejecta mass ( $M_{\text{ej}}$ ). Estimation of these parameters are crucial in understanding the explosion properties. The explosion parameters can be derived employing either detailed hydrodynamical modelling of both the light-curve and the spectra or using semi-analytical models. In the present study, several semi-analytical formulations were used to fit the quasi-bolometric light curve (see Section 3.4) of SN 2017iro.

#### 5.3.1. Estimation of $^{56}\text{Ni}$ mass, ejecta mass and kinetic energy

The optically thick phase of the light curve (photospheric phase), was fitted by the formulation originally proposed by Arnett (1982) and later updated by Valenti

et al. (2008). Major assumptions in this analytical approach comprise a small radius of the progenitor, spherical symmetry and homologous expansion of the ejecta, constant opacity ( $\kappa_{\text{opt}}$ ) and a centrally located and unmixed  $^{56}\text{Ni}$  (see Arnett 1982; Valenti et al. 2008; Cano 2013). The parameters  $M_{\text{Ni}}$  (nickel mass) and  $\tau_m$  (diffusion time-scale) were kept as free variables while obtaining the fit. Considering a uniform density medium, the ejecta kinetic energy  $E_k$  and  $\tau_m$  are, given by

$$\tau_m = \sqrt{2} \left( \frac{\kappa_{\text{opt}}}{\beta c} \right)^{1/2} \left( \frac{M_{\text{ej}}}{v_{\text{ph}}} \right)^{1/2}, \quad (1)$$

$$E_k \approx \frac{3}{5} \frac{M_{\text{ej}} v_{\text{ph}}^2}{2}, \quad (2)$$

where  $\beta \approx 13.8$  is a constant of integration (Arnett 1982) and  $c$  is the speed of light. The optical opacity  $\kappa_{\text{opt}}$  is adopted as  $0.07 \text{ cm}^2 \text{ g}^{-1}$  (e.g. Chugai 2000; Toy et al. 2016; Taddia et al. 2018). The quasi-bolometric light-curve of SN 2017iro until 30 d from the explosion epoch was fitted using least-square optimization. The best fit was obtained for a  $M_{\text{Ni}} = 0.09 \pm 0.04 M_{\odot}$  and  $\tau_m = 9.95 \pm 0.44 \text{ d}$ . The derived  $^{56}\text{Ni}$  mass was further estimated using the bolometric rise time of 16.5 d and a peak bolometric luminosity  $\log_{10} L = 42.39 \text{ erg s}^{-1}$ . The relation given by Stritzinger & Leibundgut (2005) gives a value of  $0.10 \pm 0.01 M_{\odot}$ . Using the measured Fe II line velocity  $9000 \text{ km s}^{-1}$  near the bolometric maximum (see Section 4.1), the  $M_{\text{ej}}$  and  $E_k$  are estimated as  $1.39 M_{\odot}$  and  $0.75 \times 10^{51} \text{ erg}$ , respectively.

While investigating the physical parameters of SN 2002ap, Vinkó et al. (2004) proposed analytic models for post-maximum phase with assumptions as described in the beginning of this sub-section. In brief, these models are based on the ejecta density configuration characterized by  $x_0$  (fractional radius of the core) and  $n$  (power-law exponent) parameters. We used their model C1 which represents a ‘core-shell’ structure with a fixed density core of fractional radius,  $x_0 = 0.15$  and a fixed value of  $\kappa_{\gamma} = 0.027 \text{ cm}^2 \text{ g}^{-1}$  for grey atmospheres (Sutherland & Wheeler 1984). The best-fit model is shown in Fig. 13 with an  $M_{\text{ej}} = 4.3 M_{\odot}$ ,  $M_{\text{Ni}} = 0.05 M_{\odot}$ ,  $E_k = 1.85 \text{ foe}$  and  $v_{\text{max}} = 8,500 \text{ km s}^{-1}$ .

Energy production rates of  $^{56}\text{Ni} \rightarrow ^{56}\text{Co} \rightarrow ^{56}\text{Fe}$  decay chain computed by Nadyozhin (1994) were further used to examine the mass of synthesized  $^{56}\text{Ni}$  during the explosion. The energy production curves for three different values (i.e. 0.06, 0.10, and 0.15  $M_{\odot}$ ) of the mass of  $^{56}\text{Ni}$  were over-plotted in Fig. 13. The maximum in the quasi-bolometric light curve describes roughly the transition between the emission deficit due to the large optical depth (larger diffusion timescale) and an excess emission due to the stored radiation post-maximum. The early post-maximum decline can be approximated by the instantaneous energy production rate of  $^{56}\text{Ni} \rightarrow ^{56}\text{Co}$  decay. Hence, we infer that a 0.10  $M_{\odot}$  of  $^{56}\text{Ni}$  was synthe-

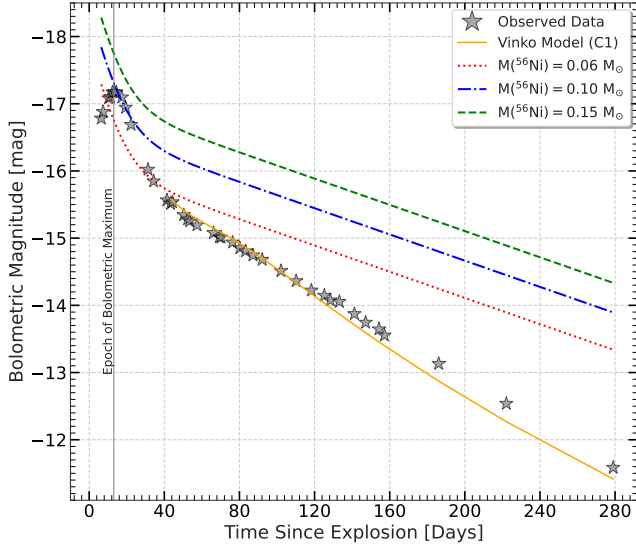


**Figure 13.** The quasi-bolometric light curve of SN 2017iro fitted with analytical model C1 of Vinkó et al. (2004). Three curves (dotted, dashed, and dash-dotted) representing the rate of energy production for different masses of  $^{56}\text{Ni}$  synthesized during the explosion, based on the analytical formulation by Nadyozhin (1994) have also been shown.

sised in the explosion due to its best-match to the initial post-maximum decline of the quasi-bolometric light-curve of SN 2017iro. The large discrepancy between the energy production rate and the quasi-bolometric luminosity during the late phase is arising due to the escape of gamma-rays.

Based upon a study of 38 SE-SNe, Lyman et al. (2016) proposed a fitting relation to estimate  $M_{\text{Ni}}$  (see their Eq. 4). To populate this data sample, we collected 9 additional SE-SNe (5 I Ib, 2 BL-Ic, 1 Ic-transitional, and 1 Ib events) with well-sampled light curves from the literature (see Table 7). Also, to estimate  $M_{\text{bol}}$ , the data available only in the optical wavelength was used. In Fig. 14, a correlation between  $M_{\text{bol}}$  and  $^{56}\text{Ni}$  mass is shown for all the 47 events. The plot also indicates that among the population of SE-SNe that the Type I Ib events produce a lesser amount of  $^{56}\text{Ni}$ . However, there appears to be no significant difference in  $^{56}\text{Ni}$  production between Type Ib and Ic SNe, whereas Type Ic-BL SNe, in general, are brighter with higher  $^{56}\text{Ni}$  mass. This is in line with other recent studies (Anderson 2019; Prentice et al. 2019). With a  $M_{\text{bol,peak}}$  of  $-17.19 \pm 0.22$  mag (cf. Table 5) and  $^{56}\text{Ni}$  mass of  $0.08 M_{\odot}$  (average value estimated from above methods), SN 2017iro (shown with a star symbol in the Fig. 14) lies near the expected correlation for SE-SNe. It is to be noted here that the explosion parameters inferred using empirical relations are approximate, and detailed hydrodynamical modelling (e.g. Taddia et al. 2018) would be required for better estimates.

**Table 7.** In addition to Lyman et al. (2016) following events are used to estimate correlation between  $M_{\text{bol}}$  and  $^{56}\text{Ni}$  mass (see Section 5.3).

Name	Type	$M_{\text{bol}}$ (mag)	$^{56}\text{Ni}$ mass ( $M_{\odot}$ )	References
SN 2011ei	I Ib	-15.8	$0.03 \pm 0.01$	1
SN 2011fu	I Ib	-17.5	$0.21 \pm 0.02$	2
SN 2012ap	Ic-BL	-17.2	$0.12 \pm 0.02$	3
SN 2012au	Ib	-17.8	$0.26 \pm 0.04$	4, 5, 6
SN 2013df	I Ib	-16.2	$0.10 \pm 0.03$	7, 8
SN 2014ad	Ic-BL	-18.1	$0.27 \pm 0.06$	9
SN 2015as	I Ib	-16.7	$0.08 \pm 0.01$	10
SN 2016coi	Ic/Ic-BL*	-16.9	$0.11 \pm 0.01$	11
SN 2016gkg	I Ib	-17.4	$0.09 \pm 0.01$	12

References: <sup>1</sup> (Milisavljevic et al. 2013b), <sup>2</sup> (Kumar et al. 2013), <sup>3</sup> (Milisavljevic et al. 2015), <sup>4</sup> (Milisavljevic et al. 2013a), <sup>5</sup> (Pandey et al. 2021), <sup>6</sup> (Takaki et al. 2013), <sup>7</sup> (Morales-Garoffolo et al. 2014), <sup>8</sup> (Szalai et al. 2016), <sup>9</sup> (Sahu et al. 2018), <sup>10</sup> (Gangopadhyay et al. 2018), <sup>11</sup> (Kumar et al. 2018), <sup>12</sup> (Tartaglia et al. 2017b).

\* Ic/Ic-BL transitional event.

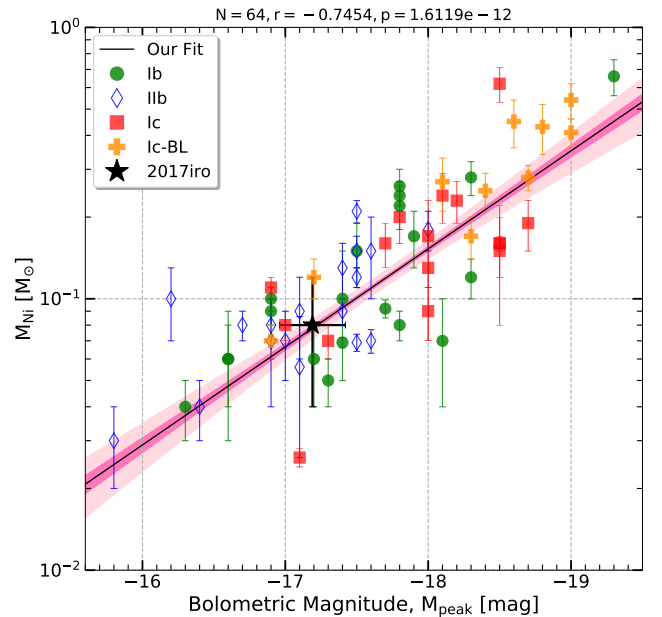


**Figure 14.** Correlation between  $M_{\text{bol}}$  and  $^{56}\text{Ni}$  mass of 47 SE-SNe (including the sample from Lyman et al. (2016) and 9 additional events, see Section 5.3). Type Ib, Ic, Ic-BL and I Ib are shown with different symbols. The bold continuous line is best fit. The dark-pink and light-pink shaded regions are indicative of  $1\sigma$  and  $3\sigma$  confidence intervals of the fit, respectively.

### 5.3.2. Oxygen mass

The [O I] line flux in the nebular spectra of SE-SNe can be used to estimate the neutral oxygen mass that is required to produce the emission. In the high electron density ( $n_e \geq 10^{-6} \text{ cm}^{-3}$ ) region, the minimum O mass can be estimated by the relation  $M_{\text{O}} = 10^8 \times D^2 \times F([\text{OI}]) \times \exp(2.28/T_4)$ , provided by Uo-



**Table 8.** Oxygen mass of Type Ib SNe.

Name	Oxygen mass ( $M_{\odot}$ )	References
SN 1996N	0.11 – 0.21	1
SN 2007Y	0.20	2
SN 2009jf	1.34	3
iPTF13bvn	0.33	4
MOT*	0.90	5
SN 2017iro	0.35	This study

\* Master OT J120451.50+265946.6

References: <sup>1</sup> (Sollerman et al. 1998), <sup>2</sup> (Stritzinger et al. 2009), <sup>3</sup> (Sahu et al. 2011), <sup>4</sup> (Kuncharayakti et al. 2015b), <sup>5</sup> (Singh et al. 2019)

moto (1986). Here, mass of neutral oxygen is represented as  $M_O$  (in  $M_{\odot}$ ),  $D$  is the SN distance (in Mpc),  $F([\text{O I}])$  is the observed absolute flux of  $[\text{O I}]$  line (in  $\text{erg s}^{-1} \text{cm}^{-2}$ ) and  $T_4$  is the temperature associated with oxygen-emitting region in units of  $10^4$  K. The  $[\text{O I}]$  5577 / (6300, 6364) line ratio can be used as a proxy for estimating the temperature. In our nebular phase spectra (cf. Fig. 9), the  $[\text{O I}]$  5577 Å line is not detected, allowing us to set  $\sim 0.1$  as the upper limit for the line ratio. At this limit, the emitting region should either be at a relatively low temperature ( $T_4 \leq 0.4$ ) for the high density limit or be at a low electron density ( $n_e \leq 5 \times 10^6 \text{ cm}^{-3}$ ) if  $T_4 = 1$  (Maeda et al. 2007a).

Previous studies have shown that during the nebular phase, the temperature of the line emitting region lies in the range 3400–4200 K (Schlegel & Kirshner 1989; Elmhamdi et al. 2004; Elmhamdi 2011). Assuming that the high-density regime is valid for SN 2017iro, the temperature of the line emitting region can be taken to be  $T_4 = 0.4$ . Using the  $[\text{O I}]$  flux (in the +209 d spectrum) of  $1.12 \times 10^{-14} \text{ erg s}^{-1} \text{cm}^{-2}$ ,  $D = 30.8$  Mpc and  $T_4 = 0.4$ , we calculated the minimum mass of neutral oxygen to be  $0.35 M_{\odot}$ , which is similar to the mass estimated for supernova iPTF13bvn (Kuncharayakti et al. 2015b). It is to be noted that for different densities, the temperature of line emitting regions may vary (Schlegel & Kirshner 1989; Leibundgut et al. 1991; Sollerman et al. 1998; Elmhamdi et al. 2004; Maeda et al. 2007a). An increase in temperature from 4000 K to 4200 K lowers the oxygen mass by a factor of  $\sim 0.8$ . Similarly, a decrease in temperature from 4000 K to 3400 K results in higher oxygen mass by a factor of  $\sim 3$ . Hence, depending on the assumed temperature and density, the range of oxygen mass spans  $0.28 - 1.05 M_{\odot}$ . The clumpy nature of the ejecta and the presence of non-optically thin material (which is not accounted here) may raise this value (Maeda et al. 2007b; Kuncharayakti et al. 2015b). In Table 8, the neutral oxygen mass estimates are listed for a few well-studied objects showing a broad range of estimated masses. We admit that the mass of the oxygen estimated here is a lower limit of the total oxygen present in the ejecta of SN 2017iro.

#### 5.4. Nature of the progenitor star

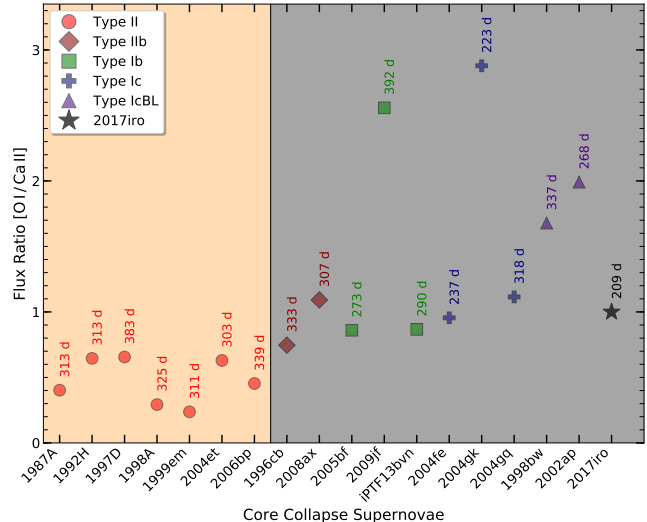


**Figure 15.**  $[\text{O I}]$  6300, 6364 /  $[\text{Ca II}]$  7291, 7324 Å line ratio of CCSNe from Kuncharayakti et al. (2015b). The  $[\text{O I}] / [\text{Ca II}]$  ratio for SN 2017iro obtained from the nebular spectra (between +173 to +209 d) has been shown with a star symbol. The phases (relative to the time of maximum light) are shown next to the each data point. The left (orange) and right (grey) regions belong to Type II and SE-SNe, respectively. The reference for spectrum are the following: SNe 1987A (Pun et al. 1995), 1992H (Clocchiatti et al. 1996), 1997D (Benetti et al. 2001), 1998A (Pastorello et al. 2005), 1998bw (Patat et al. 2001), 1999em (Leonard et al. 2002), 2004et (Sahu et al. 2006), 2004gq (Maeda et al. 2008b), 2005bf (Maeda et al. 2007c), 2006bp (Quimby et al. 2007), 1996cb, 2002ap, 2004fe, 2004gk, 2008ax, 2009jf (Modjaz et al. 2008b, 2014b).

Hydrodynamic explosion models suggest that Mg and O should have similar spatial distribution within the SN ejecta of SE-SNe (Maeda et al. 2006). Taubenberger et al. (2009) analyzed a large number of nebular spectra of SE-SNe and inferred that in a majority of cases, the line profiles of semi-forbidden Mg I] 4571 Å and forbidden oxygen  $[\text{O I}]$  6300, 6364 Å are similar, confirming the similar distribution of Mg and O in the ejecta. The strength of Mg I] 4571 Å line grows over time in comparison with  $[\text{Ca II}]$  7291, 7324 Å and  $[\text{O I}]$  because the deeper Mg-O layer of the progenitor core becomes visible with time (Foley et al. 2003; Kuncharayakti et al. 2015b). SN 2017iro shows a feeble presence of Mg I] 4571 Å possibly due to less stripping of its progenitor.

The progenitor mass of a CCSN can be constrained by estimating the  $[\text{O I}]$  6300, 6364 /  $[\text{Ca II}]$  7291, 7324 Å emission line ratio in the nebular phase (Kuncharayakti et al. 2015b). In contrast to Ca, the explosively synthesized O is sensitive to the main sequence mass of the progenitor, and therefore, a larger value implies a larger core mass (however, mixing can also play a substantial role, see Fransson & Chevalier 1989). Kuncharayakti

et al. (2015b) compared the [O I]/[Ca II] line ratio of SE-SNe and Type II SNe. They found that the line ratio of Type Ib/c SNe exhibits considerable dispersion. The observed spread in the line ratio can not be explained by the temporal evolution of the line flux. Instead, it could arise from two different progenitor channels for SE-SNe: a single massive star or a less massive star in a binary system. The [O I]/[Ca II] ratio in the spectra of SN 2017iro obtained between 173 to 209 d stays almost constant around 1. In Fig. 15, the [O I]/[Ca II] ratio of CCSNe (from Kuncarayakti et al. (2015b)) is plotted where SN 2017iro is shown with a star symbol. It indicates that the progenitor of SN 2017iro is comparatively a less massive star in a binary system. A less massive progenitor in a binary system has been proposed in several Type Ib supernovae such as SN 2007Y (Stritzinger et al. 2009), iPTF13bvn (Bersten et al. 2014b; Kuncarayakti et al. 2015b; Eldridge et al. 2015b). This is in agreement with the fact that binary interaction is a favoured scenario in a majority ( $\geq 70\%$ ) of massive stars (Podsiadlowski et al. 1992; Sana et al. 2012).

The nucleosynthesis calculations for zero-age sequence progenitor masses of 13, 15, 20, and 25  $M_{\odot}$  was performed by Thielemann, Nomoto, & Hashimoto (1996), and the corresponding oxygen mass was estimated as 0.22, 0.43, 1.48, and 3.00  $M_{\odot}$ , respectively. Limongi & Chieffi (2003) also computed explosive yields of massive stars in the mass range 13–35  $M_{\odot}$  with an initial solar composition using the FRANEC (Chieffi et al. 1998) code. Their estimated oxygen mass is  $\sim 0.3$  and  $\sim 0.5$   $M_{\odot}$  for 13 and 15  $M_{\odot}$  progenitor masses, respectively. Both the nucleosynthesis calculations indicate that the estimated oxygen mass of 0.35  $M_{\odot}$  could be produced by a progenitor star with zero-age main sequence mass in the range  $\sim 13$ –15  $M_{\odot}$ . It is further supported by the findings of Fang et al. (2019), where the upper limit of the Type IIb/Ib SNe progenitors is proposed as  $\sim 17$   $M_{\odot}$  for a progenitor in a binary system (see, also Taddia et al. 2018; Prentice et al. 2019). It is worth mentioning that the estimated oxygen mass for SN 2017iro (Section 5.3.2) is only a lower limit of the total oxygen mass. With the increased uncertainty range (0.28–1.05  $M_{\odot}$ ), the range of possible progenitor masses increases substantially, especially towards the higher progenitor masses ( $\sim 20$   $M_{\odot}$ ). However, the lower value of [O I]/[Ca II] ratio indicates towards a lower zero-age main sequence mass progenitor of SN 2017iro.

The pre-explosion images of NGC 5480 available in the HST archive (observed on 2017 January 17, Proposal ID: 14840, PI: Andrea Bellini), were examined to identify the possible progenitor candidate of SN 2017iro. The image was obtained with ACS/WFC in filter F606W. A diffuse source with an extent of 5 pixels was detected in the pre-explosion images at the supernova location. At the adopted distance of the host galaxy, the extent corresponds to  $\sim 35$  parsecs. This extended source

could possibly be a star cluster hosting the progenitor of SN 2017iro.

## 6. SUMMARY

We have presented optical photometric (40 epochs) and spectroscopic (34 epochs) follow-up of the Type Ib SN 2017iro. The light curve evolution in *UBVRI* follows the usual trend of SE-SNe, i.e., blue pass-bands peak before the red pass-bands indicating that the SN photosphere is rapidly cooling. The  $\Delta m_{15}$  parameter (for *BVRI*-bands) are comparable to those estimated for a large SE-SNe sample (Drout et al. 2011; Taddia et al. 2018) and in particular to SN 2012au. Further, the colours of SN 2017iro evolve similar to Type Ib events. The absolute *V*-band and bolometric ( $\log_{10}L$ ) luminosities are  $-17.76$  mag and  $42.39$  erg  $s^{-1}$ , respectively, indicative of a moderately luminous SN. The explosion parameters were computed by applying different analytical models to the quasi-bolometric light curve which yield a  $^{56}\text{Ni}$  mass of  $\sim 0.05$ – $0.10$   $M_{\odot}$ ,  $M_{\text{ej}}$  of  $\sim 1.4$ – $4.3$   $M_{\odot}$  and  $E_k \sim 0.8$ – $1.9 \times 10^{51}$  erg.

There seem to be two groups of Type Ib SNe in terms of the light curve tail decline rates, suggesting a heterogeneity (Wheeler et al. 2015) in the late time light curve evolution. However, lack of an adequate amount of data during the late phase of these events could be a possible reason for such inference. Hence, late phase monitoring of a larger sample of such events may provide a clearer insight to this finding. The late phase light curves of SN 2017iro decayed with moderate steepness, indicating incomplete  $\gamma$ -ray trapping by the SN ejecta. A low to moderate level of  $^{56}\text{Ni}$  mixing is supported by the non-monotonic evolution of colour curves (Dessart et al. 2012; Yoon et al. 2019) in the case of SN 2017iro. However, we can not draw a firm conclusion due to unavailability of sufficient early phase data of this event.

In the first optical spectrum ( $-7$  d) of SN 2017iro, the He I 5876 Å feature is clearly identified. Other He I lines such as 4471, 6678, and 7065 Å are comparatively weak in the beginning, but they never became as strong as He I 5876 Å. The ejecta velocity estimated using the Fe II 5169 Å line is  $\sim 9000$  km  $s^{-1}$  near *B*-band maximum which became almost constant to  $\sim 5500$  km  $s^{-1}$  beyond  $+25$  d. The Mg I line is very weak during the nebular phase in SN 2017iro. The general spectroscopic behaviour of SN 2017iro is similar to SN 2009jf and iPTF13bvn. The metallicity near SN 2017iro location ( $12 + \log(\text{O}/\text{H}) = 8.64$ ) is similar to the solar value. A neutral oxygen mass of  $\sim 0.35$   $M_{\odot}$  was estimated in the ejecta. The [O I]/[Ca II] line ratio observed in SN 2017iro indicates the progenitor had a main sequence mass of  $\sim 13$ – $15$   $M_{\odot}$ . The inferred neutral oxygen mass and the progenitor main sequence mass for SN 2017iro are very similar to the type Ib supernova iPTF13bvn that occurred in a binary system.

## ACKNOWLEDGMENTS

We thank the referee for critical review and constructive suggestions that helped to improve the paper. We also thank Sung-Chul Yoon and Hanindyo Kuncarayakti for sharing the data. BK, DKS, and GCA acknowledge BRICS grant DST/IMRCD/BRICS/PilotCall1/MuMeSTU/2017(G) for the present work. DKS and GCA also acknowledge DST/JSPS grant, DST/INT/JSPS/P/281/2018. We are grateful to the observers at HCT who provided their valuable time to monitor this event and also thank the staff of IAO, Hanle, and CREST, Hosakote,

that made these observations possible. The Weizmann interactive supernova data repository (WiSeREP) - <http://wiserep.weizmann.ac.il> is also acknowledged. This research has made use of the NASA/IPAC Extragalactic Database (NED), which is operated by the Jet Propulsion Laboratory, California Institute of Technology, under contract with the National Aeronautics and Space Administration. This research made use of REDPIPE<sup>2</sup> (Singh 2021), an assemblage of data reduction and analysis scripts written by AS.

## REFERENCES

- Anderson, J. P. 2019, *A&A*, 628, A7, doi: [10.1051/0004-6361/201935027](https://doi.org/10.1051/0004-6361/201935027)
- Anderson, J. P., Haberman, S. M., James, P. A., & Hamuy, M. 2012, *MNRAS*, 424, 1372, doi: [10.1111/j.1365-2966.2012.21324.x](https://doi.org/10.1111/j.1365-2966.2012.21324.x)
- Arcavi, I., Gal-Yam, A., Yaron, O., et al. 2011, *ApJL*, 742, L18, doi: [10.1088/2041-8205/742/2/L18](https://doi.org/10.1088/2041-8205/742/2/L18)
- Arcavi, I., Hosseinzadeh, G., Brown, P. J., et al. 2017, *ApJL*, 837, L2, doi: [10.3847/2041-8213/aa5be1](https://doi.org/10.3847/2041-8213/aa5be1)
- Arnett, W. D. 1982, *ApJ*, 253, 785, doi: [10.1086/159681](https://doi.org/10.1086/159681)
- Asplund, M., Grevesse, N., Sauval, A. J., & Scott, P. 2009, *ARA&A*, 47, 481, doi: [10.1146/annurev.astro.46.060407.145222](https://doi.org/10.1146/annurev.astro.46.060407.145222)
- Barbon, R., Benetti, S., Cappellaro, E., et al. 1995, *A&AS*, 110, 513
- Barbon, R., Benetti, S., Cappellaro, E., Rosino, L., & Turatto, M. 1990, *A&A*, 237, 79
- Benetti, S., Turatto, M., Balberg, S., et al. 2001, *MNRAS*, 322, 361, doi: [10.1046/j.1365-8711.2001.04122.x](https://doi.org/10.1046/j.1365-8711.2001.04122.x)
- Benetti, S., Turatto, M., Valenti, S., et al. 2011, *MNRAS*, 411, 2726, doi: [10.1111/j.1365-2966.2010.17873.x](https://doi.org/10.1111/j.1365-2966.2010.17873.x)
- Bersten, M. C., Tanaka, M., Tominaga, N., Benvenuto, O. G., & Nomoto, K. 2013, *ApJ*, 767, 143, doi: [10.1088/0004-637X/767/2/143](https://doi.org/10.1088/0004-637X/767/2/143)
- Bersten, M. C., Benvenuto, O. G., Folatelli, G., et al. 2014a, *AJ*, 148, 68, doi: [10.1088/0004-6256/148/4/68](https://doi.org/10.1088/0004-6256/148/4/68)
- . 2014b, *AJ*, 148, 68, doi: [10.1088/0004-6256/148/4/68](https://doi.org/10.1088/0004-6256/148/4/68)
- Bertrand, E. 2017, *Transient Name Server Classification Report*, 2017-1555, 1
- Bianco, F. B., Modjaz, M., Hicken, M., et al. 2014, *ApJS*, 213, 19, doi: [10.1088/0067-0049/213/2/19](https://doi.org/10.1088/0067-0049/213/2/19)
- Cano, Z. 2013, *MNRAS*, 434, 1098, doi: [10.1093/mnras/stt1048](https://doi.org/10.1093/mnras/stt1048)
- Cano, Z., Maeda, K., & Schulze, S. 2014, *MNRAS*, 438, 2924, doi: [10.1093/mnras/stt2400](https://doi.org/10.1093/mnras/stt2400)
- Cao, Y., Kasliwal, M. M., Arcavi, I., et al. 2013, *ApJL*, 775, L7, doi: [10.1088/2041-8205/775/1/L7](https://doi.org/10.1088/2041-8205/775/1/L7)
- Cardelli, J. A., Clayton, G. C., & Mathis, J. S. 1989, *ApJ*, 345, 245, doi: [10.1086/167900](https://doi.org/10.1086/167900)
- Chieffi, A., Limongi, M., & Straniero, O. 1998, *ApJ*, 502, 737, doi: [10.1086/305921](https://doi.org/10.1086/305921)
- Chugai, N. N. 2000, *Astronomy Letters*, 26, 797, doi: [10.1134/1.1331160](https://doi.org/10.1134/1.1331160)
- Clocchiatti, A., & Wheeler, J. C. 1997, *ApJ*, 491, 375, doi: [10.1086/304961](https://doi.org/10.1086/304961)
- Clocchiatti, A., Benetti, S., Wheeler, J. C., et al. 1996, *AJ*, 111, 1286, doi: [10.1086/117874](https://doi.org/10.1086/117874)
- Conti, P. S. 1975, *Memoires of the Societe Royale des Sciences de Liege*, 9, 193
- Couch, S. M., Pooley, D., Wheeler, J. C., & Milosavljević, M. 2011, *ApJ*, 727, 104, doi: [10.1088/0004-637X/727/2/104](https://doi.org/10.1088/0004-637X/727/2/104)
- Crowther, P. A. 2007, *ARA&A*, 45, 177, doi: [10.1146/annurev.astro.45.051806.110615](https://doi.org/10.1146/annurev.astro.45.051806.110615)
- Dessart, L., & Hillier, D. J. 2005, *A&A*, 439, 671, doi: [10.1051/0004-6361:20053217](https://doi.org/10.1051/0004-6361:20053217)
- Dessart, L., Hillier, D. J., Li, C., & Woosley, S. 2012, *MNRAS*, 424, 2139, doi: [10.1111/j.1365-2966.2012.21374.x](https://doi.org/10.1111/j.1365-2966.2012.21374.x)
- Dessart, L., Hillier, D. J., Woosley, S., et al. 2015, *MNRAS*, 453, 2189, doi: [10.1093/mnras/stv1747](https://doi.org/10.1093/mnras/stv1747)
- . 2016, *MNRAS*, 458, 1618, doi: [10.1093/mnras/stw418](https://doi.org/10.1093/mnras/stw418)
- Drout, M. R., Soderberg, A. M., Gal-Yam, A., et al. 2011, *ApJ*, 741, 97, doi: [10.1088/0004-637X/741/2/97](https://doi.org/10.1088/0004-637X/741/2/97)
- Eldridge, J. J., Fraser, M., Maund, J. R., & Smartt, S. J. 2015a, *MNRAS*, 446, 2689, doi: [10.1093/mnras/stu2197](https://doi.org/10.1093/mnras/stu2197)
- . 2015b, *MNRAS*, 446, 2689, doi: [10.1093/mnras/stu2197](https://doi.org/10.1093/mnras/stu2197)
- Eldridge, J. J., Fraser, M., Smartt, S. J., Maund, J. R., & Crockett, R. M. 2013, *MNRAS*, 436, 774, doi: [10.1093/mnras/stt1612](https://doi.org/10.1093/mnras/stt1612)
- Elmhamdi, A. 2011, *AcA*, 61, 179. <https://arxiv.org/abs/1109.2318>

<sup>2</sup> <https://github.com/sPaMFouR/RedPipe>

- Elmhamdi, A., Danziger, I. J., Cappellaro, E., et al. 2004, *A&A*, 426, 963, doi: [10.1051/0004-6361:20041318](https://doi.org/10.1051/0004-6361:20041318)
- Ensmann, L. M., & Woosley, S. E. 1988, *ApJ*, 333, 754, doi: [10.1086/166785](https://doi.org/10.1086/166785)
- Fang, Q., Maeda, K., Kuncarayakti, H., Sun, F., & Gal-Yam, A. 2019, *Nat Astron*, 3, 434, doi: [10.1038/s41550-019-0710-6](https://doi.org/10.1038/s41550-019-0710-6)
- Filippenko, A. V. 1988, *AJ*, 96, 1941, doi: [10.1086/114940](https://doi.org/10.1086/114940)
- . 1997, *ARA&A*, 35, 309, doi: [10.1146/annurev.astro.35.1.309](https://doi.org/10.1146/annurev.astro.35.1.309)
- Filippenko, A. V., Matheson, T., & Ho, L. C. 1993, *ApJL*, 415, L103, doi: [10.1086/187043](https://doi.org/10.1086/187043)
- Folatelli, G., Van Dyk, S. D., Kuncarayakti, H., et al. 2016, *ApJL*, 825, L22, doi: [10.3847/2041-8205/825/2/L22](https://doi.org/10.3847/2041-8205/825/2/L22)
- Foley, R. J., Papenkova, M. S., Swift, B. J., et al. 2003, *PASP*, 115, 1220, doi: [10.1086/378242](https://doi.org/10.1086/378242)
- Fransson, C., & Chevalier, R. A. 1989, *ApJ*, 343, 323, doi: [10.1086/167707](https://doi.org/10.1086/167707)
- Fremling, C., Sollerman, J., Taddia, F., et al. 2014, *A&A*, 565, A114, doi: [10.1051/0004-6361/201423884](https://doi.org/10.1051/0004-6361/201423884)
- . 2016, *A&A*, 593, A68, doi: [10.1051/0004-6361/201628275](https://doi.org/10.1051/0004-6361/201628275)
- Gal-Yam, A. 2017, *Observational and Physical Classification of Supernovae* (Springer International Publishing), 195–237
- Galbany, L., Stanishev, V., Mourão, A. M., et al. 2016, *A&A*, 591, A48, doi: [10.1051/0004-6361/201528045](https://doi.org/10.1051/0004-6361/201528045)
- Gangopadhyay, A., Misra, K., Pastorello, A., et al. 2018, *MNRAS*, 476, 3611, doi: [10.1093/mnras/sty478](https://doi.org/10.1093/mnras/sty478)
- Graur, O., Bianco, F. B., Huang, S., et al. 2017a, *ApJ*, 837, 120, doi: [10.3847/1538-4357/aa5eb8](https://doi.org/10.3847/1538-4357/aa5eb8)
- Graur, O., Bianco, F. B., Modjaz, M., et al. 2017b, *ApJ*, 837, 121, doi: [10.3847/1538-4357/aa5eb7](https://doi.org/10.3847/1538-4357/aa5eb7)
- Groh, J. H., Georgy, C., & Ekström, S. 2013a, *A&A*, 558, L1, doi: [10.1051/0004-6361/201322369](https://doi.org/10.1051/0004-6361/201322369)
- . 2013b, *A&A*, 558, L1, doi: [10.1051/0004-6361/201322369](https://doi.org/10.1051/0004-6361/201322369)
- Hachisu, I., Matsuda, T., Nomoto, K., & Shige-yama, T. 1991, *ApJL*, 368, L27, doi: [10.1086/185940](https://doi.org/10.1086/185940)
- Hamuy, M., Maza, J., Pinto, P. A., et al. 2002, *AJ*, 124, 417, doi: [10.1086/340968](https://doi.org/10.1086/340968)
- Harkness, R. P., Wheeler, J. C., Margon, B., et al. 1987, *ApJ*, 317, 355, doi: [10.1086/165283](https://doi.org/10.1086/165283)
- Heger, A., Fryer, C. L., Woosley, S. E., Langer, N., & Hartmann, D. H. 2003, *ApJ*, 591, 288, doi: [10.1086/375341](https://doi.org/10.1086/375341)
- Kamble, A., Soderberg, A. M., Chomiuk, L., et al. 2014, *ApJ*, 797, 2, doi: [10.1088/0004-637X/797/1/2](https://doi.org/10.1088/0004-637X/797/1/2)
- Kilpatrick, C. D., Foley, R. J., Abramson, L. E., et al. 2017, *MNRAS*, 465, 4650, doi: [10.1093/mnras/stw3082](https://doi.org/10.1093/mnras/stw3082)
- Kilpatrick, C. D., Takaro, T., Foley, R. J., et al. 2018, *MNRAS*, 480, 2072, doi: [10.1093/mnras/sty2022](https://doi.org/10.1093/mnras/sty2022)
- Kilpatrick, C. D., Drout, M. R., Achetttl, K., et al. 2021, *MNRAS*, 504, 2073, doi: [10.1093/mnras/stab838](https://doi.org/10.1093/mnras/stab838)
- Kumar, B., Singh, A., Srivastav, S., Sahu, D. K., & Anupama, G. C. 2018, *MNRAS*, 473, 3776, doi: [10.1093/mnras/stx2498](https://doi.org/10.1093/mnras/stx2498)
- Kumar, B., Pandey, S. B., Sahu, D. K., et al. 2013, *MNRAS*, 431, 308, doi: [10.1093/mnras/stt162](https://doi.org/10.1093/mnras/stt162)
- Kuncarayakti, H., Maeda, K., Bersten, M. C., et al. 2015a, *A&A*, 579, A95, doi: [10.1051/0004-6361/201425604](https://doi.org/10.1051/0004-6361/201425604)
- . 2015b, *A&A*, 579, A95, doi: [10.1051/0004-6361/201425604](https://doi.org/10.1051/0004-6361/201425604)
- Landolt, A. U. 1992, *AJ*, 104, 340, doi: [10.1086/116242](https://doi.org/10.1086/116242)
- Leibundgut, B., Kirshner, R. P., Pinto, P. A., et al. 1991, *ApJ*, 372, 531, doi: [10.1086/169998](https://doi.org/10.1086/169998)
- Leonard, D. C., Filippenko, A. V., Gates, E. L., et al. 2002, *PASP*, 114, 35, doi: [10.1086/324785](https://doi.org/10.1086/324785)
- Li, W., Leaman, J., Chornock, R., et al. 2011a, *MNRAS*, 412, 1441, doi: [10.1111/j.1365-2966.2011.18160.x](https://doi.org/10.1111/j.1365-2966.2011.18160.x)
- . 2011b, *MNRAS*, 412, 1441, doi: [10.1111/j.1365-2966.2011.18160.x](https://doi.org/10.1111/j.1365-2966.2011.18160.x)
- Limongi, M., & Chieffi, A. 2003, *ApJ*, 592, 404, doi: [10.1086/375703](https://doi.org/10.1086/375703)
- Liu, Y.-Q., Modjaz, M., Bianco, F. B., & Graur, O. 2016, *ApJ*, 827, 90, doi: [10.3847/0004-637X/827/2/90](https://doi.org/10.3847/0004-637X/827/2/90)
- Lucy, L. B. 1991, *ApJ*, 383, 308, doi: [10.1086/170787](https://doi.org/10.1086/170787)
- Lyman, J. D., Bersier, D., James, P. A., et al. 2016, *MNRAS*, 457, 328, doi: [10.1093/mnras/stv2983](https://doi.org/10.1093/mnras/stv2983)
- Maeda, K., Mazzali, P. A., & Nomoto, K. 2006, *ApJ*, 645, 1331, doi: [10.1086/504581](https://doi.org/10.1086/504581)
- Maeda, K., Tanaka, M., Nomoto, K., et al. 2007a, *ApJ*, 666, 1069, doi: [10.1086/520054](https://doi.org/10.1086/520054)
- Maeda, K., Kawabata, K., Tanaka, M., et al. 2007b, *ApJL*, 658, L5, doi: [10.1086/513564](https://doi.org/10.1086/513564)
- Maeda, K., Tanaka, M., Nomoto, K., et al. 2007c, *ApJ*, 666, 1069, doi: [10.1086/520054](https://doi.org/10.1086/520054)
- Maeda, K., Kawabata, K., Mazzali, P. A., et al. 2008a, *Science*, 319, 1220, doi: [10.1126/science.1149437](https://doi.org/10.1126/science.1149437)
- . 2008b, *Science*, 319, 1220, doi: [10.1126/science.1149437](https://doi.org/10.1126/science.1149437)
- Malesani, D., Fynbo, J. P. U., Hjorth, J., et al. 2009, *ApJL*, 692, L84, doi: [10.1088/0004-637X/692/2/L84](https://doi.org/10.1088/0004-637X/692/2/L84)
- Massey, P. 2003, *ARA&A*, 41, 15, doi: [10.1146/annurev.astro.41.071601.170033](https://doi.org/10.1146/annurev.astro.41.071601.170033)
- Maund, J. R., Smartt, S. J., Kudritzki, R. P., Podsiadlowski, P., & Gilmore, G. F. 2004, *Nature*, 427, 129, doi: [10.1038/nature02161](https://doi.org/10.1038/nature02161)
- Maund, J. R., Wheeler, J. C., Baade, D., et al. 2009, *ApJ*, 705, 1139, doi: [10.1088/0004-637X/705/2/1139](https://doi.org/10.1088/0004-637X/705/2/1139)

- Maund, J. R., Fraser, M., Ergon, M., et al. 2011, *ApJL*, 739, L37, doi: [10.1088/2041-8205/739/2/L37](https://doi.org/10.1088/2041-8205/739/2/L37)
- Mazzali, P. A., Kawabata, K. S., Maeda, K., et al. 2005, *Science*, 308, 1284, doi: [10.1126/science.1111384](https://doi.org/10.1126/science.1111384)
- Mazzali, P. A., Valenti, S., Della Valle, M., et al. 2008, *Science*, 321, 1185, doi: [10.1126/science.1158088](https://doi.org/10.1126/science.1158088)
- Milisavljevic, D., Fesen, R. A., Gerardy, C. L., Kirshner, R. P., & Challis, P. 2010, *ApJ*, 709, 1343, doi: [10.1088/0004-637X/709/2/1343](https://doi.org/10.1088/0004-637X/709/2/1343)
- Milisavljevic, D., Patnaude, D. J., Chevalier, R. A., et al. 2018, *ApJL*, 864, L36, doi: [10.3847/2041-8213/aadd4e](https://doi.org/10.3847/2041-8213/aadd4e)
- Milisavljevic, D., Soderberg, A. M., Margutti, R., et al. 2013a, *ApJL*, 770, L38, doi: [10.1088/2041-8205/770/2/L38](https://doi.org/10.1088/2041-8205/770/2/L38)
- Milisavljevic, D., Margutti, R., Soderberg, A. M., et al. 2013b, *ApJ*, 767, 71, doi: [10.1088/0004-637X/767/1/71](https://doi.org/10.1088/0004-637X/767/1/71)
- Milisavljevic, D., Margutti, R., Parrent, J. T., et al. 2015, *ApJ*, 799, 51, doi: [10.1088/0004-637X/799/1/51](https://doi.org/10.1088/0004-637X/799/1/51)
- Minkowski, R. 1941, *PASP*, 53, 224, doi: [10.1086/125315](https://doi.org/10.1086/125315)
- Modjaz, M., Gutiérrez, C. P., & Arcavi, I. 2019, *Nature Astronomy*, 3, 717, doi: [10.1038/s41550-019-0856-2](https://doi.org/10.1038/s41550-019-0856-2)
- Modjaz, M., Kewley, L., Bloom, J. S., et al. 2011, *ApJL*, 731, L4, doi: [10.1088/2041-8205/731/1/L4](https://doi.org/10.1088/2041-8205/731/1/L4)
- Modjaz, M., Kirshner, R. P., Blondin, S., Challis, P., & Matheson, T. 2008a, *ApJL*, 687, L9, doi: [10.1086/593135](https://doi.org/10.1086/593135)
- . 2008b, *ApJL*, 687, L9, doi: [10.1086/593135](https://doi.org/10.1086/593135)
- Modjaz, M., Li, W., Butler, N., et al. 2009a, *ApJ*, 702, 226, doi: [10.1088/0004-637X/702/1/226](https://doi.org/10.1088/0004-637X/702/1/226)
- . 2009b, *ApJ*, 702, 226, doi: [10.1088/0004-637X/702/1/226](https://doi.org/10.1088/0004-637X/702/1/226)
- Modjaz, M., Blondin, S., Kirshner, R. P., et al. 2014a, *AJ*, 147, 99, doi: [10.1088/0004-6256/147/5/99](https://doi.org/10.1088/0004-6256/147/5/99)
- . 2014b, *AJ*, 147, 99, doi: [10.1088/0004-6256/147/5/99](https://doi.org/10.1088/0004-6256/147/5/99)
- Morales-Garoffolo, A., Elias-Rosa, N., Benetti, S., et al. 2014, *MNRAS*, 445, 1647, doi: [10.1093/mnras/stu1837](https://doi.org/10.1093/mnras/stu1837)
- Morales-Garoffolo, A., Elias-Rosa, N., Bersten, M., et al. 2015, *MNRAS*, 454, 95, doi: [10.1093/mnras/stv1972](https://doi.org/10.1093/mnras/stv1972)
- Mould, J. R., Huchra, J. P., Freedman, W. L., et al. 2000, *ApJ*, 529, 786, doi: [10.1086/308304](https://doi.org/10.1086/308304)
- Nadyozhin, D. K. 1994, *ApJS*, 92, 527, doi: [10.1086/192008](https://doi.org/10.1086/192008)
- Nicholl, M. 2018, *Research Notes of the American Astronomical Society*, 2, 230, doi: [10.3847/2515-5172/aaf799](https://doi.org/10.3847/2515-5172/aaf799)
- Nomoto, K. 1984, *ApJ*, 277, 791, doi: [10.1086/161749](https://doi.org/10.1086/161749)
- . 1987, *ApJ*, 322, 206, doi: [10.1086/165716](https://doi.org/10.1086/165716)
- Nomoto, K. I., Iwamoto, K., & Suzuki, T. 1995, *PhR*, 256, 173, doi: [10.1016/0370-1573\(94\)00107-E](https://doi.org/10.1016/0370-1573(94)00107-E)
- Pandey, S. B., Kumar, A., Kumar, B., et al. 2021, *arXiv e-prints*, arXiv:2106.15856. <https://arxiv.org/abs/2106.15856>
- Pastorello, A., Baron, E., Branch, D., et al. 2005, *MNRAS*, 360, 950, doi: [10.1111/j.1365-2966.2005.09079.x](https://doi.org/10.1111/j.1365-2966.2005.09079.x)
- Pastorello, A., Kasliwal, M. M., Crockett, R. M., et al. 2008, *MNRAS*, 389, 955, doi: [10.1111/j.1365-2966.2008.13618.x](https://doi.org/10.1111/j.1365-2966.2008.13618.x)
- Patat, F., Cappellaro, E., Danziger, J., et al. 2001, *ApJ*, 555, 900, doi: [10.1086/321526](https://doi.org/10.1086/321526)
- Pauldrach, A. W. A., Vanbeveren, D., & Hoffmann, T. L. 2012, *A&A*, 538, A75, doi: [10.1051/0004-6361/201117621](https://doi.org/10.1051/0004-6361/201117621)
- Perlmutter, S., Pennypacker, C., Graham, J. R., & Soifer, B. T. 1988, *IAUC*, 4590, 1
- Pettini, M., & Pagel, B. E. J. 2004, *MNRAS*, 348, L59, doi: [10.1111/j.1365-2966.2004.07591.x](https://doi.org/10.1111/j.1365-2966.2004.07591.x)
- Phillips, M. M. 1993, *ApJL*, 413, L105, doi: [10.1086/186970](https://doi.org/10.1086/186970)
- Phillips, M. M., Simon, J. D., Morrell, N., et al. 2013, *ApJ*, 779, 38, doi: [10.1088/0004-637X/779/1/38](https://doi.org/10.1088/0004-637X/779/1/38)
- Piro, A. L., & Nakar, E. 2013, *ApJ*, 769, 67, doi: [10.1088/0004-637X/769/1/67](https://doi.org/10.1088/0004-637X/769/1/67)
- Podsiadlowski, P., Joss, P. C., & Hsu, J. J. L. 1992, *ApJ*, 391, 246, doi: [10.1086/171341](https://doi.org/10.1086/171341)
- Podsiadlowski, P., Langer, N., Poelarends, A. J. T., et al. 2004, *ApJ*, 612, 1044, doi: [10.1086/421713](https://doi.org/10.1086/421713)
- Pols, O. R., & Dewi, J. D. M. 2002, *PASA*, 19, 233, doi: [10.1071/AS01121](https://doi.org/10.1071/AS01121)
- Poznanski, D., Ganeshalingam, M., Silverman, J. M., & Filippenko, A. V. 2011, *MNRAS*, 415, L81, doi: [10.1111/j.1745-3933.2011.01084.x](https://doi.org/10.1111/j.1745-3933.2011.01084.x)
- Poznanski, D., Prochaska, J. X., & Bloom, J. S. 2012, *MNRAS*, 426, 1465, doi: [10.1111/j.1365-2966.2012.21796.x](https://doi.org/10.1111/j.1365-2966.2012.21796.x)
- Prabhu, T. P. 2014, *Proceedings of the Indian National Science Academy Part A*, 80, 887, doi: [10.16943/ptinsa/2014/v80i4/55174](https://doi.org/10.16943/ptinsa/2014/v80i4/55174)
- Prentice, S. J., Mazzali, P. A., Pian, E., et al. 2016, *MNRAS*, 458, 2973, doi: [10.1093/mnras/stw299](https://doi.org/10.1093/mnras/stw299)
- Prentice, S. J., Ashall, C., James, P. A., et al. 2019, *MNRAS*, 485, 1559, doi: [10.1093/mnras/sty3399](https://doi.org/10.1093/mnras/sty3399)
- Puls, J., Vink, J. S., & Najarro, F. 2008, *A&A Rv*, 16, 209, doi: [10.1007/s00159-008-0015-8](https://doi.org/10.1007/s00159-008-0015-8)
- Pun, C. S. J., Kirshner, R. P., Sonneborn, G., et al. 1995, *ApJS*, 99, 223, doi: [10.1086/192185](https://doi.org/10.1086/192185)
- Quimby, R. M., Wheeler, J. C., Höflich, P., et al. 2007, *ApJ*, 666, 1093, doi: [10.1086/520532](https://doi.org/10.1086/520532)
- Richardson, D., Branch, D., & Baron, E. 2006, *AJ*, 131, 2233, doi: [10.1086/500578](https://doi.org/10.1086/500578)
- Richmond, M. W., Treffers, R. R., Filippenko, A. V., et al. 1994, *AJ*, 107, 1022, doi: [10.1086/116915](https://doi.org/10.1086/116915)
- Roming, P. W. A., Pritchard, T. A., Brown, P. J., et al. 2009, *ApJL*, 704, L118, doi: [10.1088/0004-637X/704/2/L118](https://doi.org/10.1088/0004-637X/704/2/L118)

- Roy, R., Kumar, B., Maund, J. R., et al. 2013, MNRAS, 434, 2032, doi: [10.1093/mnras/stt1148](https://doi.org/10.1093/mnras/stt1148)
- Ryder, S. D., Van Dyk, S. D., Fox, O. D., et al. 2018, ApJ, 856, 83, doi: [10.3847/1538-4357/aaaf1e](https://doi.org/10.3847/1538-4357/aaaf1e)
- Sahu, D. K., Anupama, G. C., Chakradhari, N. K., et al. 2018, MNRAS, 475, 2591, doi: [10.1093/mnras/stx3212](https://doi.org/10.1093/mnras/stx3212)
- Sahu, D. K., Anupama, G. C., Srividya, S., & Muneer, S. 2006, MNRAS, 372, 1315, doi: [10.1111/j.1365-2966.2006.10937.x](https://doi.org/10.1111/j.1365-2966.2006.10937.x)
- Sahu, D. K., Gurugubelli, U. K., Anupama, G. C., & Nomoto, K. 2011, MNRAS, 413, 2583, doi: [10.1111/j.1365-2966.2011.18326.x](https://doi.org/10.1111/j.1365-2966.2011.18326.x)
- Sana, H., de Mink, S. E., de Koter, A., et al. 2012, Science, 337, 444, doi: [10.1126/science.1223344](https://doi.org/10.1126/science.1223344)
- Sánchez, S. F., Kennicutt, R. C., Gil de Paz, A., et al. 2012, A&A, 538, A8, doi: [10.1051/0004-6361/201117353](https://doi.org/10.1051/0004-6361/201117353)
- Sanders, N. E., Soderberg, A. M., Levesque, E. M., et al. 2012, ApJ, 758, 132, doi: [10.1088/0004-637X/758/2/132](https://doi.org/10.1088/0004-637X/758/2/132)
- Schlafly, E. F., & Finkbeiner, D. P. 2011, ApJ, 737, 103, doi: [10.1088/0004-637X/737/2/103](https://doi.org/10.1088/0004-637X/737/2/103)
- Schlafly, E. F., Meisner, A. M., Stutz, A. M., et al. 2016, ApJ, 821, 78, doi: [10.3847/0004-637X/821/2/78](https://doi.org/10.3847/0004-637X/821/2/78)
- Schlegel, E. M., & Kirshner, R. P. 1989, AJ, 98, 577, doi: [10.1086/115158](https://doi.org/10.1086/115158)
- Shahbandeh, M., Hsiao, E. Y., Ashall, C., et al. 2021, arXiv e-prints, arXiv:2110.12083, <https://arxiv.org/abs/2110.12083>
- Shigeyama, T., Nomoto, K., Tsujimoto, T., & Hashimoto, M.-A. 1990, ApJL, 361, L23, doi: [10.1086/185818](https://doi.org/10.1086/185818)
- Shivvers, I., Filippenko, A. V., Silverman, J. M., et al. 2019, MNRAS, 482, 1545, doi: [10.1093/mnras/sty2719](https://doi.org/10.1093/mnras/sty2719)
- Singh, A. 2021, RedPipe: Reduction Pipeline, <http://ascl.net/2106.024>
- Singh, M., Misra, K., Sahu, D. K., et al. 2019, MNRAS, 485, 5438, doi: [10.1093/mnras/stz752](https://doi.org/10.1093/mnras/stz752)
- Smartt, S. J. 2009, ARA&A, 47, 63, doi: [10.1146/annurev-astro-082708-101737](https://doi.org/10.1146/annurev-astro-082708-101737)
- Smith, N. 2006, ApJ, 644, 1151, doi: [10.1086/503766](https://doi.org/10.1086/503766)
- . 2014a, ARA&A, 52, 487, doi: [10.1146/annurev-astro-081913-040025](https://doi.org/10.1146/annurev-astro-081913-040025)
- . 2014b, ARA&A, 52, 487, doi: [10.1146/annurev-astro-081913-040025](https://doi.org/10.1146/annurev-astro-081913-040025)
- Smith, N., & Owocki, S. P. 2006, ApJL, 645, L45, doi: [10.1086/506523](https://doi.org/10.1086/506523)
- Soderberg, A. M., Berger, E., Page, K. L., et al. 2008, Nature, 453, 469, doi: [10.1038/nature06997](https://doi.org/10.1038/nature06997)
- Sollerman, J., Leibundgut, B., & Spyromilio, J. 1998, A&A, 337, 207
- Srivastav, S., Anupama, G. C., & Sahu, D. K. 2014, MNRAS, 445, 1932, doi: [10.1093/mnras/stu1878](https://doi.org/10.1093/mnras/stu1878)
- Stalin, C. S., Hegde, M., Sahu, D. K., et al. 2008, in Astron. Soc. India Conf. Ser., 36, 111, <https://arxiv.org/abs/0809.1745>
- Stritzinger, M., & Leibundgut, B. 2005, A&A, 431, 423, doi: [10.1051/0004-6361:20041630](https://doi.org/10.1051/0004-6361:20041630)
- Stritzinger, M., Hamuy, M., Suntzeff, N. B., et al. 2002, AJ, 124, 2100, doi: [10.1086/342544](https://doi.org/10.1086/342544)
- Stritzinger, M., Mazzali, P., Phillips, M. M., et al. 2009, ApJ, 696, 713, doi: [10.1088/0004-637X/696/1/713](https://doi.org/10.1088/0004-637X/696/1/713)
- Stritzinger, M. D., Taddia, F., Burns, C. R., et al. 2018, A&A, 609, A135, doi: [10.1051/0004-6361/201730843](https://doi.org/10.1051/0004-6361/201730843)
- Stritzinger, M. D., Taddia, F., Holmbo, S., et al. 2020, A&A, 634, A21, doi: [10.1051/0004-6361/201936619](https://doi.org/10.1051/0004-6361/201936619)
- Sutherland, P. G., & Wheeler, J. C. 1984, ApJ, 280, 282, doi: [10.1086/161995](https://doi.org/10.1086/161995)
- Swartz, D. A. 1991, ApJ, 373, 604, doi: [10.1086/170079](https://doi.org/10.1086/170079)
- Szalai, T., Vinkó, J., Nagy, A. P., et al. 2016, MNRAS, 460, 1500, doi: [10.1093/mnras/stw1031](https://doi.org/10.1093/mnras/stw1031)
- Taddia, F., Sollerman, J., Leloudas, G., et al. 2015, A&A, 574, A60, doi: [10.1051/0004-6361/201423915](https://doi.org/10.1051/0004-6361/201423915)
- Taddia, F., Stritzinger, M. D., Bersten, M., et al. 2018, A&A, 609, A136, doi: [10.1051/0004-6361/201730844](https://doi.org/10.1051/0004-6361/201730844)
- Takaki, K., Kawabata, K. S., Yamanaka, M., et al. 2013, ApJL, 772, L17, doi: [10.1088/2041-8205/772/2/L17](https://doi.org/10.1088/2041-8205/772/2/L17)
- Takáts, K., & Vinkó, J. 2012, MNRAS, 419, 2783, doi: [10.1111/j.1365-2966.2011.19921.x](https://doi.org/10.1111/j.1365-2966.2011.19921.x)
- Tartaglia, L., Fraser, M., Sand, D. J., et al. 2017a, ApJL, 836, L12, doi: [10.3847/2041-8213/aa5c7f](https://doi.org/10.3847/2041-8213/aa5c7f)
- . 2017b, ApJL, 836, L12, doi: [10.3847/2041-8213/aa5c7f](https://doi.org/10.3847/2041-8213/aa5c7f)
- Taubenberger, S., Valenti, S., Benetti, S., et al. 2009, MNRAS, 397, 677, doi: [10.1111/j.1365-2966.2009.15003.x](https://doi.org/10.1111/j.1365-2966.2009.15003.x)
- Theureau, G., Hanski, M. O., Coudreau, N., Hallet, N., & Martin, J. M. 2007, A&A, 465, 71, doi: [10.1051/0004-6361:20066187](https://doi.org/10.1051/0004-6361:20066187)
- Thielemann, F.-K., Nomoto, K., & Hashimoto, M.-A. 1996, ApJ, 460, 408, doi: [10.1086/176980](https://doi.org/10.1086/176980)
- Toy, V. L., Cenko, S. B., Silverman, J. M., et al. 2016, ApJ, 818, 79, doi: [10.3847/0004-637X/818/1/79](https://doi.org/10.3847/0004-637X/818/1/79)
- Turatto, M., Benetti, S., & Cappellaro, E. 2003, in Proc. ESO-MPA-MPE Workshop, From Twilight to Highlight: The Physics of Supernovae. Springer, Berlin, p. 200, ed. W. Hillebrandt & B. Leibundgut
- Uomoto, A. 1986, ApJL, 310, L35, doi: [10.1086/184777](https://doi.org/10.1086/184777)
- Vacca, W. D., & Leibundgut, B. 1996, ApJL, 471, L37, doi: [10.1086/310323](https://doi.org/10.1086/310323)
- Valenti, S., Benetti, S., Cappellaro, E., et al. 2008, MNRAS, 383, 1485, doi: [10.1111/j.1365-2966.2007.12647.x](https://doi.org/10.1111/j.1365-2966.2007.12647.x)
- Valenti, S., Fraser, M., Benetti, S., et al. 2011, MNRAS, 416, 3138, doi: [10.1111/j.1365-2966.2011.19262.x](https://doi.org/10.1111/j.1365-2966.2011.19262.x)

- Van Dyk, S. D., Zheng, W., Clubb, K. I., et al. 2013, *ApJL*, 772, L32, doi: [10.1088/2041-8205/772/2/L32](https://doi.org/10.1088/2041-8205/772/2/L32)
- Van Dyk, S. D., Zheng, W., Brink, T. G., et al. 2018, *ApJ*, 860, 90, doi: [10.3847/1538-4357/aac32c](https://doi.org/10.3847/1538-4357/aac32c)
- Vinkó, J., Blake, R. M., Sárneczky, K., et al. 2004, *A&A*, 427, 453, doi: [10.1051/0004-6361:20040272](https://doi.org/10.1051/0004-6361:20040272)
- Wellstein, S., & Langer, N. 1999, *A&A*, 350, 148.  
<https://arxiv.org/abs/astro-ph/9904256>
- Wellstein, S., Langer, N., & Braun, H. 2001, *A&A*, 369, 939, doi: [10.1051/0004-6361:20010151](https://doi.org/10.1051/0004-6361:20010151)
- Wheeler, J. C., Johnson, V., & Clocchiatti, A. 2015, *MNRAS*, 450, 1295, doi: [10.1093/mnras/stv650](https://doi.org/10.1093/mnras/stv650)
- Wheeler, J. C., & Levreault, R. 1985, *ApJL*, 294, L17, doi: [10.1086/184500](https://doi.org/10.1086/184500)
- Wiggins, P. 2017, *Transient Name Server Discovery Report*, 2017-1354, 1
- Williamson, M., Modjaz, M., & Bianco, F. B. 2019, *ApJL*, 880, L22, doi: [10.3847/2041-8213/ab2edb](https://doi.org/10.3847/2041-8213/ab2edb)
- Woosley, S. E., & Eastman, R. G. 1997, in *NATO Advanced Science Institutes (ASI) Series C*, Vol. 486, *NATO Advanced Science Institutes (ASI) Series C*, ed. P. Ruiz-Lapuente, R. Canal, & J. Isern, 821, doi: [10.1007/978-94-011-5710-0\\_51](https://doi.org/10.1007/978-94-011-5710-0_51)
- Woosley, S. E., Langer, N., & Weaver, T. A. 1995, *ApJ*, 448, 315, doi: [10.1086/175963](https://doi.org/10.1086/175963)
- Woosley, S. E., & Weaver, T. A. 1995, *ApJS*, 101, 181, doi: [10.1086/192237](https://doi.org/10.1086/192237)
- Xiang, D., Wang, X., Mo, J., et al. 2019, *ApJ*, 871, 176, doi: [10.3847/1538-4357/aaf8b0](https://doi.org/10.3847/1538-4357/aaf8b0)
- Yoon, S.-C. 2015a, *PASA*, 32, e015, doi: [10.1017/pasa.2015.16](https://doi.org/10.1017/pasa.2015.16)
- . 2015b, *PASA*, 32, e015, doi: [10.1017/pasa.2015.16](https://doi.org/10.1017/pasa.2015.16)
- Yoon, S.-C., Chun, W., Tolstov, A., Blinnikov, S., & Dessart, L. 2019, *ApJ*, 872, 174, doi: [10.3847/1538-4357/ab0020](https://doi.org/10.3847/1538-4357/ab0020)
- Yoon, S.-C., Woosley, S. E., & Langer, N. 2010, *ApJ*, 725, 940, doi: [10.1088/0004-637X/725/1/940](https://doi.org/10.1088/0004-637X/725/1/940)